

Thermodynamic properties for applications in chemical industry via classical force fields

Gabriela Guevara-Carrion, Hans Hasse and Jadran Vrabec

Abstract Thermodynamic properties of fluids are of key importance for the chemical industry. Presently, the fluid property models used in classical process design and optimization are mostly equations of state or G^E models, which are parameterized using experimental data. Molecular modeling and simulation based on classical force fields is a promising alternative route, which in many cases reasonably complements the well established methods. The present contribution gives an introduction to the state-of-the-art in this field regarding molecular models, simulation methods and tools. Attention is given to the way modeling and simulation on the scale of molecular force fields interacts with other scales, which is mainly by parameter inheritance. Parameters for molecular force fields are determined both bottom-up from quantum chemistry and top-down from experimental data. Commonly used functional forms for describing the intra- and intermolecular interactions are presented. Several approaches for *ab initio* to empirical force field parameterization are discussed. Some transferable force field families, which are frequently used in chemical engineering applications, are described. Furthermore, some examples of force fields that were parameterized for specific molecules are given. Molecular dynamics and Monte Carlo methods for the calculation of transport properties and vapor-liquid equilibria are introduced. Two case studies are presented: First, using liquid ammonia as an example, the capabilities of semi-empirical force fields, parameterized on the basis of quantum chemical information and experimental data, are discussed with respect to thermodynamic properties that are relevant for the chemical industry. Second, the ability of molecular simulation methods to accurately describe vapor-liquid equilibrium properties of binary mixtures containing CO₂ is shown.

Gabriela Guevara-Carrion · Hans Hasse
Laboratory of Engineering Thermodynamics, Erwin-Schrödinger-Strasse 44, 67663 Kaiserslautern
e-mail: hans.hasse@mv.uni-kl.de

Jadran Vrabec*
Thermodynamics and Energy Technology, Warburger Strasse 100, 33098 Paderborn e-mail: jadran.vrabec@upb.de

1 Introduction

The knowledge of thermodynamic properties plays a crucial role in the design and operation of chemical plants [1]. Therefore, the chemical industry requires reliable and accurate thermodynamic data for very different fluids, covering a wide range of temperature, pressure and composition [1, 2, 3, 4, 5, 6]. There is a great demand for data on vapor-liquid, liquid-liquid and solid-liquid equilibria, as well as an increasing need for caloric and transport properties [1]. Classical approaches to predict these properties like equations of state and G^E models, as reviewed e.g. by Poling et al. [7], do exist. However, the parameters of these models are determined based on experimental data. These are often not available and may be difficult to obtain, especially for extreme conditions or when hazardous substances are involved. Furthermore, as the amount of experimental data is always limited, usually extrapolations are necessary, but they are inherently uncertain. Therefore, an alternative route to determine fluid properties, independent of the established phenomenological approaches, is highly desirable. This would allow carrying out predictions in different ways and, if the results agree, give confidence or, in the opposite case, give a warning regarding the quality of the extrapolation.

Moreover, most processes in the chemical industry are governed by nanoscale phenomena. In many cases the nanoscale structure plays an important role, e.g. the local concentrations and not the overall concentrations govern reactions at active sites of catalysts. Phenomenological thermodynamics provides no route to obtain insight in these nanoscale structures and processes, whereas molecular simulations based on forces fields do. The key is to carry them out with models that are suitably developed and reasonably represent the compounds.

Molecular modeling and simulation comprises computational techniques derived from quantum chemistry and statistical mechanics to predict equilibrium and non-equilibrium properties of molecular ensembles based on intra- and intermolecular interaction potentials. Because of the ongoing exponential increase in computing power and the development of new numerical methods, the range of molecules that can be covered and the accuracy of the results is growing rapidly [8]. Nowadays, molecular modeling and simulation is being actively applied in physical, chemical and biological sciences as well as in engineering research and its importance will further increase [1, 9]. The development of new molecular theories as well as the prediction of material properties as a function of molecular structure and thermodynamic conditions are other examples of current applications of molecular methods. Moreover, molecular simulation can also provide insight into the molecular behavior and properties which are not experimentally accessible.

One of the central issues of the molecular approach is to devise adequate force fields that accurately describe the properties of real systems. Depending on the application field, different requirements need to be fulfilled. In biology, for instance, to study protein folding in aqueous environments, typically rather complex force fields are used to determine microscopic molecular structures. In the chemical industry, much more aggregated macroscopic properties are needed, but the quantitative correctness of the data is essential.

Simulation results are primarily determined by the employed force field. Fortunately, in the past two decades, the quality of force fields has greatly improved, mainly due to the inclusion of molecular parameters obtained from high-level *ab initio* calculations [10]. The aim of this contribution is to review the current status of force field development and application for the prediction of thermodynamic properties of fluids that are relevant for the chemical industry.

2 Force Fields

The development of force fields comprises a trade-off between computational feasibility and coverage of the molecular interactions details and is thus driven by the growth of computational resources [9].

Force fields are a set of mathematical functions and parameters that relate a potential energy to a configuration of the regarded molecular system. The potential energy is usually described by pair potentials. Three- and more-body interactions do contribute significantly to the potential energy as well [11], but are usually not explicitly included in engineering force fields because of their high computational cost. Rather, their contributions are incorporated into pairwise approximations by effective pair potentials [11].

In molecular force fields, the interaction energy between sites can be divided into contributions from intramolecular and intermolecular interactions. The significance of the different contributions to the force field varies depending on the required application. E.g., for industrial engineering applications, simple models with a low computational cost are required that are nonetheless able to accurately predict thermodynamic properties. Numerous force fields of varying complexity are currently available. The simplest force fields include only potentials that describe the intermolecular interactions and are frequently used for small molecules. More complex force fields include intramolecular interactions that are necessary for the simulation of larger molecules such as polymers.

All-atom force fields consider every atom as an individual interaction site, while united-atom force fields gather different atoms of a functional group into one interaction site, e.g. as it is often done to model methyl or methylene groups. To describe chain-like polymers or proteins, also coarse grained force fields are employed, where the interaction sites usually represent a larger number of atoms.

2.1 Intermolecular Interactions

In modeling with classical force fields, the intermolecular interactions are usually divided into: Van der Waals interactions (repulsion and dispersion) and electrostatic interactions. In this framework, the Van der Waals interactions take into account all the interactions between sites that are not related to permanent electrostatics, such

as dispersion, repulsion and induction [12]. Hydrogen bonding is usually modeled by electrostatic sites. For a detailed discussion of the intermolecular interactions, the interested reader is referred to [13].

2.1.1 Van der Waals Interactions

The simplest potential to describe the Van der Waals interactions, neglecting attractive forces, is the hard-sphere (HS):

$$u^{\text{HS}}(r_{ij}) = \begin{cases} \infty & r_{ij} \leq \sigma \\ 0 & r_{ij} > \sigma \end{cases}, \quad (1)$$

where σ is the site diameter and r_{ij} is the site-site distance. A slightly more detailed alternative to the HS potential is the soft-sphere (SS) potential:

$$u^{\text{SS}}(r_{ij}) = \begin{cases} \zeta (\sigma/r_{ij})^v & r_{ij} \leq \sigma \\ 0 & r_{ij} > \sigma \end{cases}, \quad (2)$$

where v is a parameter usually chosen to be an integer number and ζ is a measure of the magnitude of the repulsive interaction. The square-well (SW) potential is the simplest model that considers both repulsion and attraction

$$u^{\text{SW}}(r_{ij}) = \begin{cases} \infty & r_{ij} \leq \sigma \\ -\varepsilon & \sigma < r_{ij} \leq \lambda \sigma \\ 0 & r_{ij} > \lambda \sigma \end{cases}, \quad (3)$$

where ε is a measure of the attractive interaction and λ is some multiple of the hard-sphere diameter. Another simple potential that includes a physical description of dispersion is the Sutherland potential

$$u^{\text{Su}}(r_{ij}) = \begin{cases} \infty & r_{ij} \leq \sigma \\ -\varepsilon (\sigma/r_{ij})^6 & r_{ij} > \sigma \end{cases}. \quad (4)$$

The HS, SS, SW and Sutherland potentials are highly idealized approximations that are nowadays rather used for the development of liquid state theories.

The most popular effective pair potential representing the Van der Waals interactions is the Lennard-Jones (LJ) potential, which was given in a general form by Mie [14]

$$u^{\text{Mie}}(r_{ij}) = \frac{\varepsilon}{n-m} \left(\frac{n^n}{m^m} \right)^{\frac{1}{n-m}} \left[\left(\frac{\sigma}{r_{ij}} \right)^n - \left(\frac{\sigma}{r_{ij}} \right)^m \right], \quad (5)$$

where σ and ε are the size parameter and the energy well-depth, respectively. For the dispersive term, $m = 6$ is specified because of its physical significance. For the repulsive term, with little theoretical justification, $n = 9 \cdots 16$ is usually employed. The most common form is the LJ 12-6 potential ($n = 12$, $m = 6$)

$$u^{\text{LJ}}(r_{ij}) = 4\epsilon \left[\left(\frac{\sigma}{r_{ij}} \right)^{12} - \left(\frac{\sigma}{r_{ij}} \right)^6 \right]. \quad (6)$$

The choice of the exponent $n = 12$ has rather computational than physical reasons, because it is simply the square of the dispersion term.

There are also many variations of the LJ 12-6 potential. One example is the computationally inexpensive truncated and shifted Lennard-Jones potential (TSLJ), which is commonly used for molecular simulation studies in which large molecular ensembles are regarded, e.g. for investigating condensation processes [15, 16]. Another version of the LJ potential is the Kihara potential [17], which is a non-spherical generalization of the LJ model.

One weakness of the LJ potential is the lack of a realistic description of repulsion, which originates from the Pauli exclusion principle. The Buckingham exponential-6 potential takes the actual exponential decay into account [18]

$$u^{\text{X6}}(r_{ij}) = \begin{cases} \frac{\epsilon}{1-6/\alpha} \left[\frac{6}{\alpha} \exp \left[\alpha \left(1 - \frac{r_{ij}}{R} \right) \right] - \left(\frac{R}{r_{ij}} \right)^6 \right] & r_{ij} > R_{\text{max}} \\ \infty & r_{ij} \leq R_{\text{max}} \end{cases}, \quad (7)$$

where α is the repulsive steepness factor, ϵ is the well-depth located at the distance R and R_{max} represents the distance of the potential false maximum. By definition, the Buckingham potential is set to infinity for $r_{ij} \leq R_{\text{max}}$ in order to avoid an unphysical behavior of the potential at short distances which is only due to mathematical reasons.

Another potential function that describes the dispersive forces due to instantaneous polarities arising from fluctuations in the electron clouds is the Drude model series expansion [19]

$$u^{\text{D}}(r_{ij}) = -\frac{C_{ij}^{(6)}}{r_{ij}^6} - \frac{C_{ij}^{(8)}}{r_{ij}^8} - \frac{C_{ij}^{(10)}}{r_{ij}^{10}} - \dots, \quad (8)$$

where all coefficients $C_{ij}^{(n)}$ are positive, implying an attractive interaction. The first term of the expansion considers instantaneous dipole-dipole interactions, while the higher order terms include instantaneous dipole-quadrupole, quadrupole-quadrupole, etc. interactions.

As computational resources improved, force fields were introduced which are parameterized exclusively based on *ab initio* calculations [20, 21, 22, 23, 24]. Different analytical site-site potential functions are employed, e.g. the Tang and Toennies potential [25]

$$u^{\text{TT}}(r_{ij}) = A_{ij} \exp(-\alpha_{ij} r_{ij}) - f_6 \frac{C_{ij}^{(6)}}{r_{ij}^6} - f_8 \frac{C_{ij}^{(8)}}{r_{ij}^8}. \quad (9)$$

The damping functions f_6 and f_8 account for the influence of the charge overlap on the dispersion potential in the region of the potential well and are defined by [25]

$$f_n(r_{ij}) = 1 - \exp(-b_{ij}r_{ij}) \sum_{k=0}^n \frac{(b_{ij}r_{ij})^k}{k!}, \quad (10)$$

where b_{ij} is a parameter that determines the effective damping length.

2.1.2 Combining Rules

The definition of different sites, particularly in case of mixtures, implies that interaction parameter sets for unlike site pairs are required. If sufficient data either experimental or theoretical (*ab initio*) are available, these rules can be abandoned completely. The main reason for using combining rules is to avoid a huge number of additional parameters for unlike atoms. Thus, many combining rules have been proposed, which are empirical or based on mathematical and physical intuition [26, 27, 28, 29, 30, 31]. Most of the combining rules for the LJ potential parameters rely on pure component data alone, however, some combining rules incorporate additional molecular information like polarizability, ionization potential or diamagnetic susceptibility. A review and detailed description of LJ combining rules can be found e.g. in [32, 33, 34].

Some force fields use the geometric mean (Berthelot rule) for both LJ parameters

$$\begin{aligned} \sigma_{ij} &= \sqrt{\sigma_i \sigma_j} \\ \varepsilon_{ij} &= \sqrt{\varepsilon_i \varepsilon_j}. \end{aligned} \quad (11)$$

However, by far the most commonly employed LJ combining rule is that of Lorentz [35] and Berthelot [36]

$$\begin{aligned} \sigma_{ij} &= \frac{1}{2}(\sigma_i + \sigma_j) \\ \varepsilon_{ij} &= \sqrt{\varepsilon_i \varepsilon_j}. \end{aligned} \quad (12)$$

The use of the arithmetic mean for the unlike size parameter was proposed by Lorentz motivated by the collision of hard spheres, on the other hand, the geometric mean for the unlike energy parameter was proposed with little physical argument by Berthelot. Therefore, it is not surprising that this combining rule often leads to inaccurate mixture properties [34, 37, 38].

An effective approach is to provide the Lorentz-Berthelot combining rule with at least one extra parameter that can be adjusted to some experimental data of the mixture. A modification that is adequate for the description for the unlike LJ parameters for vapor-liquid equilibria [34] is

$$\begin{aligned}\sigma_{ij} &= \frac{1}{2}(\sigma_i + \sigma_j) \\ \varepsilon_{ij} &= \xi \sqrt{\varepsilon_i \varepsilon_j}.\end{aligned}\quad (13)$$

This modified rule was successfully applied to vapor-liquid equilibria of numerous mixtures [39, 40, 41]. Here, the binary parameter ξ was adjusted to one experimental data point for vapor pressure or Henry's law constant of the studied binary mixture.

2.1.3 Electrostatic Interactions

The electrostatic interactions of ionic and polar molecules in the form of charges or multipoles contribute significantly to the potential energy. For an exact description of a typical charge distribution, a large set of electric moments is required [42]. However, often just dipoles and quadrupoles are taken into account, since they are usually the most significant [19]. Because the multipole expansion at one site converges slowly, an alternative approach is to distribute fictitious point charges, dipoles or quadrupoles throughout the molecule to cover the multipole moments [11, 43].

Electrostatic interactions can also be represented by a distribution of point charges, an approach used in numerous force fields. Both representations (point charges and atomic multipoles) are strictly valid only at long range. The electrostatic interaction which acts between a pair of point charges q_i and q_j is described by Coulomb's law:

$$u^{qq}(r_{ij}) = \frac{1}{4\pi\varepsilon_0} \frac{q_i q_j}{r_{ij}}, \quad (14)$$

where $\varepsilon_0 = 8.854187817 \cdot 10^{-12}$ F/m is the permittivity of the vacuum.

The interaction potential between two dipoles μ_i and μ_j is

$$u^{\mu\mu}(r_{ij}, \boldsymbol{\omega}_i, \boldsymbol{\omega}_j) = \frac{1}{4\pi\varepsilon_0} \frac{\mu_i \mu_j}{r_{ij}^3} \cdot f^{\mu\mu}(\boldsymbol{\omega}_i, \boldsymbol{\omega}_j), \quad (15)$$

and the one between two quadrupoles Q_i and Q_j is given by:

$$u^{QQ}(r_{ij}, \boldsymbol{\omega}_i, \boldsymbol{\omega}_j) = \frac{1}{4\pi\varepsilon_0} \frac{3Q_i Q_j}{4r_{ij}^5} \cdot f^{QQ}(\boldsymbol{\omega}_i, \boldsymbol{\omega}_j). \quad (16)$$

f^{QQ} and $f^{\mu\mu}$ are expressions for the dependency of the electrostatic interactions on the orientations $\boldsymbol{\omega}_i$ and $\boldsymbol{\omega}_j$ of the molecules i and j . Their definition and the potential functions acting between higher order multipoles as well as the cross-interactions between different polarities like charge-dipole or dipole-quadrupole, can be found e.g. in [44].

2.1.4 Polarization

Polarization is a response of the spatial electronic charge distribution of a molecule to an external field, e.g. induced by neighboring polar molecules [19]. The energy contribution due to polarization is accounted for by different methods, reviews on this topic can be found in [45, 46, 47]. A common approach is to include induced point dipoles for each atom [48]. An induced atomic dipole is given by [19]:

$$\boldsymbol{\mu}^{\text{ind}} = \alpha \mathbf{V}_{\mathbf{f}}, \quad (17)$$

and the interaction energy is

$$u^{\text{ind}}(\alpha, V_f) = - \int_0^{V_f} dV_{\mathbf{f}} \alpha V_{\mathbf{f}} = -\frac{1}{2} \alpha V_f^2, \quad (18)$$

where α is the atomic polarizability, which is usually assumed to be isotropic. The electric field $\mathbf{V}_{\mathbf{f}}$ is the sum of the fields due to permanent and induced dipoles acting on the atoms.

An induced dipole can also be modeled by a charge fixed to an atom to which an opposite massless movable charge is attached via a harmonic potential. This simple model is called Drude oscillator or charge-on-spring [47]. An alternative route to model polarizability is the fluctuating charge model [49]. This method uses the principle of electronegativity equalization, which ensures that atomic chemical potentials are constant throughout the molecule. Hence, the charges are fluctuating variables which respond to their environment. The charges flow between the atoms until the instantaneous electronegativities of the atoms are balanced [45]. In this context, the charges are replaced by dynamic charge distributions whose interactions are calculated by a Coulomb integral expression [19].

2.1.5 Hydrogen Bonding

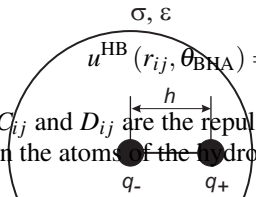
In addition to the interactions mentioned above, other types of attractive interactions can be also observed, e.g. the widespread hydrogen bond. Hydrogen bonding occurs when a hydrogen atom, which is covalently bonded to an electronegative atom A, is able to approach closely to another electronegative atom B with a relatively strong attractive interaction. A hydrogen bond can be represented as $A-H \cdots B$. Therein, A and B are usually of the chemical type O, N, S or halogens, however, also weakly electronegative atoms like C can be bonded to a H atom that acts as a proton donor, e.g. in formic acid [50].

One common approach to represent hydrogen bonding in force fields is based on point charges superimposed on LJ 12-6 sites, as e.g. in the SPC/E water model. The charges on the electronegative and hydrogen sites provide the electrostatic forces between molecules, while the Lennard-Jones interactions between electronegative sites provide short range repulsion to balance the electrostatic attraction and determine the size of the molecule. In this type of model, the hydrogen bonds are

Fig. 1 Hydrogen bonding group composed of one Lennard-Jones site (σ, ϵ) and two point charges (q_-, q_+).

purely electrostatic and arise because the hydrogen sites are near the periphery of the molecule. Figure 1 illustrates a hydrogen bonding group composed of one LJ site and two point charges. The negative point charge (q_-) coincides with the LJ site, while the positive point charge (q_+) is positioned eccentrically with a distance h to the LJ site.

Hydrogen bonds can also be explicitly modeled replacing the LJ 12-6 term between hydrogen bonding atoms by an empirical hydrogen bonding potential function that reproduces the hydrogen bonding distance and energy [19]. An example is a modification of the LJ 10-12 potential

$$u^{\text{HB}}(r_{ij}, \theta_{\text{BHA}}) = \left(\frac{C_{ij}}{r_{ij}}\right)^{12} - \left(\frac{D_{ij}}{r_{ij}}\right)^{10} \cos^4(\theta_{\text{BHA}}), \quad (19)$$


where C_{ij} and D_{ij} are the repulsive and attractive parameters and θ_{BHA} is the angle between the atoms of the hydrogen bond (A-H...B).

2.2 Intramolecular Interactions

There are several types of intramolecular interactions, also called bonded or valence interactions, which contribute to the potential energy, i.e. bond stretching, bond angle bending, dihedral angle motion, improper angle bending, etc. These are not exclusively pair interactions, but include three- and four-body interactions as well. The parameters of the intramolecular potentials are typically fitted to reproduce geometries, vibrational frequencies and energy profiles from *ab initio* calculations [9].

2.2.1 Bond Stretching

Bond stretching potentials describe the change in potential energy with the bond distance between two neighboring sites. Bond stretching is frequently represented

by a harmonic potential. Thereby, analogously to Hook's law, the sites are connected by an ideal spring

$$u_{\text{bond}}^{\text{har}}(r_{ij}) = \frac{1}{2}k_{ij}(r_{ij} - r_0)^2, \quad (20)$$

where k_{ij} is the bond stretching force constant and r_0 is a reference bond length. This reference value is not the equilibrium length, but the bond length reached when all the other force field terms are set to zero [19]. However, physically, bond stretching does not exhibit a harmonic potential. Thus, anharmonic bond stretching potentials are also used, the simplest one adds a cubic term to Eq. 20. Other examples of anharmonic potentials are the Simon-Parr-Finland potential [51] or the Morse potential [52]

$$u_{\text{bond}}^{\text{Mor}}(r_{ij}) = D[1 - \exp(-\alpha r_{ij})]^2, \quad (21)$$

where D is the energy well-depth and α is related to the stretching force constant of the bond. The Morse potential is more suitable to describe bond stretching than the simple harmonic potential [53]. Note that Eq. 20 is a good approximation of Eq. 21 in case of small r_{ij} .

2.2.2 Angle Bending

Angle bending interactions occur when an angle formed by three consecutive sites is perturbed from its equilibrium value. Several potentials are employed to describe this energy contribution, however, the majority of force fields is based on the harmonic potential [54]

$$u_{\text{angle}}^{\text{har}}(\theta) = \frac{1}{2}k_{\theta}(\theta - \theta_0)^2, \quad (22)$$

or the trigonometric potential

$$u_{\text{angle}}^{\text{cos}}(\theta) = \frac{1}{2}k_{\theta}(\cos(\theta) - \cos(\theta_0))^2, \quad (23)$$

where θ is the angle formed by three consecutive sites, cf. Figure 2, and θ_0 is its equilibrium value. The bending force constant k_{θ} is typically smaller than the bond force constant k_{ij} , because the energy required to distort an angle from its equilibrium value is lower than that required to stretch a bond [19].

2.2.3 Torsional Rotation Terms

Many of the major changes in molecular conformations are due to bond rotations. The torsion interactions account for the rotation around bonds of four adjacent sites or the motion of dihedral angles. The torsional potentials are 2π -periodic and sy-

mmetric at 0 and π . For alkanes, the Ryckaert and Belleman [55] torsional potential is often used

$$u_{\text{torsion}}^{\text{RB}}(\varphi) = \sum_n c_n \cos^n(\varphi), \quad (24)$$

where c_n are the dihedral force constants of order n . An equivalent torsional potential is based on the Fourier cosine series expansion

$$u_{\text{torsion}}^{\text{F}}(\varphi) = \sum_n \frac{1}{2} V_n (1 + \cos(n\varphi - \delta_n)), \quad (25)$$

where φ is the dihedral angle as shown in Figure 2. V_n are the torsional rotation force constants, δ_n the phase factors and n the multiplicity or number of function minima upon a rotation of 2π . The specified number of terms in the series expansion varies for different force fields. Common choices are the first three terms of the expansion and terms with selected multiplicity from one to six [53].

2.2.4 Improper Torsion

A special type of torsional potential is employed to enforce geometrical constraints like planarity, e.g. in aromatic rings, or to prevent transitions between chiral structures. This potential is usually referred to as improper torsion or out-of-plane bending. Improper torsion acts between four atoms in a branched structure. There are several approaches to describe this potential. E.g., to maintain the improper dihedral at 0 or π , the torsional potential of the form

$$u_{\text{improper}}^{2\pi}(\varphi) = V_n (1 - \cos(2\varphi)), \quad (26)$$

can be used. Another route to incorporate the out-of-plane bending motion is to define an angle ψ between a bond from the central atom and the plane defined by the central atom and the other two atoms, cf. Figure 2. With this definition, a harmonic potential can be constructed

$$u_{\text{improper}}^{\text{har}}(\psi) = \frac{1}{2} k_\psi (\psi - \psi_0)^2, \quad (27)$$

where ψ is the improper angle and ψ_0 its equilibrium value. k_ψ is a constant that determines the stiffness of the potential.

2.2.5 Valence Coordinate Cross Terms

Some force fields include cross terms to account for the coupling between different intramolecular interactions. E.g., it has been found that upon decrease of a bond angle θ , adjacent bonds stretch to reduce the interactions between the atoms forming the bond. Only few force fields include such cross terms, because it was found that

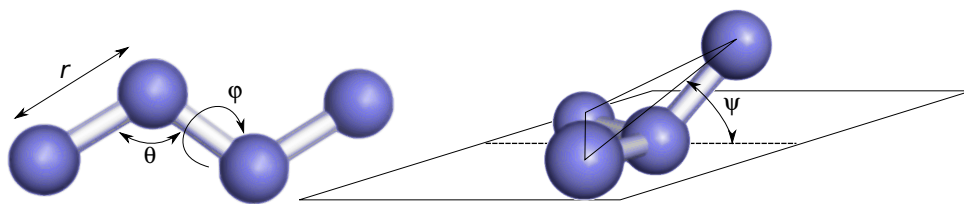


Fig. 2 Schematic representation of the intramolecular coordinates: bond length r , bending angle θ , torsional dihedral angle φ and improper dihedral angle ψ .

they are rarely important. Cross terms are usually a function of two interactions like bond-bond, bond-angle, bond-torsion or angle-torsion, but terms containing more than two interactions can be also used. Cross terms are important to cover vibrational spectra, but do not significantly affect structural or thermodynamic properties [56]. Force fields can be classified depending on whether or not they include cross terms. Various forms of cross terms can be found in [19] that are not further discussed here.

2.2.6 1-4 Interactions

Van der Waals interactions were mentioned as intermolecular interactions. However, in many force fields Van der Waals and electrostatic interactions are also used to describe the intramolecular interactions between different sites of the same molecule that are separated by three (1-4 potential) or more bonds. Usually, the intramolecular 1-4 potential is scaled for both the LJ and Coulombic contributions by an empirical factor, depending on the force field.

3 Force Field Parameterization

In the past, force fields were parameterized based only on experimental data, nowadays, most modern force fields include substantial quantum chemical information. According to the nature of the data used for parameterization, force fields can be classified as *ab initio*, semi-empirical and empirical. Simple potentials, e.g. for argon, which require few parameters, can be fitted exclusively to macroscopic experimental data, however, more complex force fields have numerous parameters and thus heavily depend on *ab initio* data. The present contribution gives an introduction to the present state-of-the-art in this field. Attention is given to the way how modeling and simulation on the scale of molecular force fields interacts with other scales, which is mainly by parameter inheritance. Parameters are determined both bottom-up from quantum chemistry and top-down from experimental data.

In principle, every quantity that can be predicted from force field calculations can also be used for its parameterization. The choice of the properties taken as optimization target may depend on the intended application. However, if the target properties

are suitably chosen, force field models often show powerful predictive capabilities. This is due to the fact that they reasonably separate the different types of intermolecular interactions and are thus able to account for the interplay of interaction energy and structure of the fluid, which is generally a weak point in phenomenological approaches. Force fields for applications in the chemical industry should be developed including data on the liquid density as well as on entropic properties, namely phase equilibria [57]. This is in line with more than 100 years experience from phenomenological thermodynamics which shows that for characterizing a pure fluid, its vapor pressure curve is of prime importance. It may, however, be desirable to also include other properties like transport coefficients in the parameter optimization. Mathematically, a multi-objective optimization problem has to be solved. However, because of parameter correlations [58], quite different parameter sets may reproduce a given set of target data with satisfactory accuracy.

There are several methods to perform a force field parameterization. In the trial and error approach, the parameters are gradually refined to better fit the target data, however, this is inefficient and difficult because of parameter coupling. It is more reasonable to use dedicated fitting algorithms to optimally describe the target data. Over the last years, numerous algorithms have been developed to facilitate automated force field parameterization on the basis of thermodynamic target properties [59, 60, 61, 62] and quantum chemical information such as energy surfaces [63, 64, 65].

3.1 *Ab Initio* Parameterization

Ab initio quantum mechanics (QM) can be used to calculate a wide range of molecular and structural properties, and additionally, to derive properties that depend on the electronic structure. *Ab initio* data from QM calculations can be employed in different stages of force field parameterization. They can be adopted directly into the force field, taken as target data or as initial values in optimization procedures and may also be used for force field validation.

Having in mind that the quality of a force field depends on the quality of the data used for optimization, a benchmark analysis of the QM calculations should be performed, because *ab initio* data are only reliable when sufficiently high levels of theory and large basis sets are used. However, such QM calculations are computationally very demanding. Therefore, with the current computer capabilities, system sizes that can be handled are limited to up to approximately 10^3 non-hydrogen atoms.

Ab initio calculations are mostly used for molecular geometries and intramolecular interaction parameters [66, 67, 68]. However, QM calculations can also be employed to determine parameters of the intermolecular potential, e.g. for the polar interactions.

3.1.1 Van der Waals Interactions

The Van der Waals interactions are not well accessible with *ab initio* methods, because the characterization of short-range intermolecular interactions requires a much higher level of theory than molecular structure or conformational energies. Moreover, at least a reasonably complete two-body interaction energy landscape is required. Thus, a large number of molecular separations and mutual orientations must be considered, which is computationally very demanding. Once the appropriate points of the energy landscape are obtained, they can be fitted to an analytical function [69]. Note that the liquid behavior is not well reproduced by *ab initio* calculations, since only small clusters can be handled [70]. A review of QM methods used for the calculation of interaction energies and potential energy sampling is given in [69].

3.1.2 Electrostatic Interactions

Electrostatic properties of molecules can be determined from the electron density distribution obtained by QM. Different methods have been proposed for this end. E.g., atomic charges can be estimated using different partitioning methods like Mulliken and Lödwin population analysis [71, 72], the charge model 2 (CM2) formalism [73], natural population analysis (NPA) [74] or the theory of atoms in molecules (AIM) [75]. A comparison of these methods for the calculation of atomic charges can be found e.g. in [76]. Atomic charges calculated by population methods are often considered to be inappropriate for force field parameterization [19]. The most common approach is to derive the atomic charges from the electrostatic potential (ESP), applying either semi-empirical density functional theory (DFT), Hartree-Fock (HF) or post HF methods [77]. The ESP is a QM observable which can be determined from wave functions. In this method, atomic charges are fitted to the calculated ESP for a series of points in a three-dimensional spatial grid surrounding the molecule. The fitting procedure is performed with the constraint that the sum of the charges equals the net charge of the molecule. The positions where the potential is evaluated, are often chosen just outside the atomic Van der Waals radii, because the accuracy of electrostatics is most important there. Different methods consider different sampling points where the ESP is calculated, i.e. the distance from the Van der Waals surface [19]. The CHELP [78] method considers spherical shells extended to 3 Å from the Van der Waals surface, whereas the CHELPG [79] method contemplates a cubic grid of points extended to 2.8 Å. A restrained electrostatic potential (RESP) [80] fit is often used to include restrictions to the obtained charges, e.g. to restrain charges in buried atoms. RESP can be employed to fit partial charges to the ESP of a single or multiple conformers [77]. There are various difficulties with the ESP fitting approach, like conformation, basis set dependency and the presence of buried atoms. The inclusion of multiple conformations in the fitting procedure can be employed to overcome these problems [81]. A comparison of some commonly applied schemes can be found in [82].

The second order Møller-Plesset (MP2) perturbation theory is often adequate in terms of accuracy and efficiency for describing the ESP [10]. It is generally considered that the 6-31G* basis set gives reasonable results [19]. This basis set results in dipole moments that are 10 to 20% larger than expected in the gas phase, which is desirable for deriving charges for liquid phase simulations [80]. More advanced *ab initio* methods, e.g. the coupled cluster method together with correlation consistent basis sets can also be used for such calculations [83].

Electrostatic multipole moments of molecules, i.e. dipoles, quadrupoles or octupoles, can also be obtained from QM wave functions. Methods like distributed multipole analysis (DMA) [84] or AIM [85] assign multipole moments to each atom or to specified sites of a molecule. The DMA method estimates multipole moments from QM wave functions and the highest obtained multipole moment depends on the basis set used. There are no limitations in this method on number or position of the multipoles, also anisotropic effects due to lone pairs or π electrons can be considered.

A simpler approach, typically employed for small symmetric molecules, is to estimate ideal point multipoles by integration over the orbitals resulting from the calculated electron density distribution. The accuracy of the calculated moments is highly dependent on the basis set, electron correlation and molecular geometry [19]. The MP2 level of theory with the 6-31G* polarizable basis set is broadly applied in such calculations. In order to save computational effort, MP2 is often executed as a single point calculation for a geometry determined on the basis of a lower level of theory.

In condensed phases, the mutual polarization of solute and solvent molecules should be considered. This can be done by placing a single molecule into a cavity that is surrounded by a dielectric continuum and assigning the dielectric constant of the liquid to it [86]. Thus, the molecule in the cavity induces polarization in the surrounding dielectric continuum, which in turn interacts with the electron density of the molecule. There are numerous techniques of varying complexity, a review can be found e.g. in [87]. One of the pioneering techniques is the self consistent reaction field (SCRF) [88, 89] approach. Some variations of this method treat the continuum solvent as a conductor, such as in the conductor-like screening model (COSMO) [90] or the polarizable continuum model (PCM) [87]. Another rather simple approach to account for condensed phase polarization is the multipole scaling procedure [80, 91].

3.1.3 Intramolecular Interactions

The geometric parameters of force fields, i.e. reference bond lengths and bond angles, are commonly assigned according to equilibrium molecular geometries determined by QM, combined with an energy minimization algorithm. The agreement between *ab initio* and experimental equilibrium geometries increases with the size of the basis set and the level of theory. However, the HF level of theory with a relative small basis set, such as 6-31G, is sufficient to obtain good results [60, 86, 92].

Fortuitously, the STO-3G basis set often performs well with respect to molecular geometry, despite its deficiencies. In general, the bond lengths predicted by the STO-3G basis set are too long, while the ones obtained with the 6-31G basis set are too short [19]. As an alternative QM approach, DFT, using gradient corrected and hybrid methods can be applied, since it is known to achieve excellent results for equilibrium geometries [10, 93]. An important example is the Becke's three-parameter density functional hybrid method combined with the Lee, Yang and Parr gradient-corrected correlation functional B3LYP [94].

QM is widely used to calculate relative energies of conformation sets and energy barriers between them. Hence, bond length, bond angle and torsional potential terms can be fitted to reproduce intramolecular energy surfaces, the relative energy of conformational pairs or rotational energy profiles. The variation of energy for different configurations can be calculated quite accurately with relatively small basis sets. The rotational energy profiles are often taken as a basis to determine the torsional interactions. For this purpose, the energy of a series of molecular structures generated by bond rotation is obtained from *ab initio* calculations. The torsional potential is fitted to the resulting energy profile together with the Van der Waals and electrostatic potentials [19]. Both HF and MP2, together with the 6-31G basis set, are often employed for such calculations [95]. It should be noted that DFT with the B3LYP functional performs rather poorly for intermolecular interactions and conformational energies [10].

3.2 Empirical Parameterization

Due to the difficulties of QM methods to correctly describe condensed phase behavior, Van der Waals parameters and atomic point charges of molecular models are often adjusted to reproduce experimental data on macroscopic properties of the liquid state. Usually, they are fitted to thermodynamic properties determined by means of molecular dynamics (MD) or Monte Carlo (MC) simulations.

3.2.1 Intermolecular Interactions

Intermolecular potential parameters can be optimized to different types of experimental data. For engineering applications, liquid density and liquid enthalpy are very often used. E.g., the liquid density strongly depends on the LJ size parameter σ , whereas the enthalpy of vaporization strongly depends on the LJ energy well depth ε [60]. Therefore, intermolecular parameters are frequently adjusted to experimental data on both of these quantities, as in the OPLS force field [96]. The vapor pressure is even more sensitive to the intermolecular potential parameters so that, particularly in recent years, it was chosen together with the saturated liquid density and the heat of vaporization to devise numerous generic force fields of interest for chemical engineers like TraPPE, AUA and NERD. The latter strategy was also used

for the development of a wide variety of specific molecular models for engineering applications [97, 98, 99].

Many other physical properties may also be taken as targets for parameter optimization of Van der Waals and electrostatic potentials: second virial coefficient [100, 101], critical temperature [102], free energy of hydration [103], self-diffusion coefficient [104, 105], shear viscosity [105, 106, 107], radial distribution functions [57, 108] or multipole moments [109].

3.2.2 Intramolecular Interactions

Equilibrium geometries of molecules can be derived from gas-phase experiments, such as electron diffraction and microwave spectroscopy [60]. Raman and infrared vibrational frequencies can also be used to determine force constants for bond stretching and angle bending. If available, experimental data on relative configuration stabilities and barrier heights can be used to parameterize torsional and improper potential terms [19].

4 Force Field Families

Numerous force fields with different degrees of sophistication are in use today, however, none of them is universally accepted. A molecular force field is generally designed and parameterized to reproduce certain properties and should be able to predict a wide range of thermodynamic properties for different thermodynamic conditions. Force fields can be transferable (using the same set of parameters to model a variety of related compounds) or specific (using distinct sets of parameters for each molecule). Beside the choice of the potential functions of the force field, another important decision is whether or not to represent all atoms explicitly. In this context, force fields can be divided into all-atom, united-atom and coarse grained types.

4.1 Transferable Force Fields

In transferable force fields, the parameters for a given functional group are deemed transferable between different molecules. There are numerous transferable force field families, which were developed for different applications. Below, some families relevant for chemical engineers are described: optimized potentials for liquid simulations (OPLS) [96, 110, 111, 112], transferable potential for phase equilibria (TraPPE) [113, 114, 115, 116, 117, 118, 119, 120, 121, 122], optimized potential model for phase equilibria (OPPE) [59, 68, 107, 123, 124, 125, 126, 127, 128, 129, 130], Nath, Escobedo and de Pablo (NERD) force field [100, 131, 132, 133] and the

GIBBS99 exponential-6 force field [18, 134], cf. Table 1. Many force fields families are continuously being improved and extended to include new types of compounds, thus numerous versions are available.

Table 1 Some important characteristics of the different united-atom force field families for alkanes.

Force field family	Van der Waals potential	Bond stretching	Angle bending	Torsional potential	Combining rule
OPLS-UA	LJ 12-6	no	no	yes	Berthelot
OPLS-UA/AMBER	LJ 12-6	yes	yes	yes	Berthelot
TraPPE	LJ 12-6	no	yes	yes	Lorentz-Berthelot
OPPE-AUA	LJ 12-6	no	yes	yes	Lorentz-Berthelot
NERD	LJ 12-6	yes	yes	yes	Lorentz-Berthelot
GIBBS99	Buckingham	no	yes	yes	Lorentz-Berthelot

4.1.1 OPLS Force Field

The optimized potentials for liquid simulations (OPLS) force field can be divided into the OPLS-UA (united-atom) [96, 110, 111, 112] and the OPLS-AA (all-atom) [57, 67, 92, 103, 135, 136, 137, 138, 139] versions. Among the two, the OPLS-UA force field is predominantly used for engineering applications, mainly because it is computationally cheaper than the all-atom version. The OPLS-UA force field is available for hydrocarbons [96], amides [110], peptides [110], alcohols [111] or proteins [112]. The OPLS-AA force field was parameterized for small organic molecules and is intended for biochemical applications. The parameters of the OPLS-AA force field are available for a broader range of functional groups and molecules. Thus, besides hydrocarbons [103] and alcohols [57], parameters can be found for thiols [57], sulfides [57], ketones [57], amides [57], amines [139], pyrrole [138], furan [138], diazoles [138], oxazoles [138], proteins [67], carbohydrates [92], among others.

The functional forms of both OPLS force field families are similar. In the original OPLS-UA force field, the only intramolecular degrees of freedom that were taken into account were torsions. Later on, the OPLS-UA force field was merged with the description of bond stretching and angle bending from the AMBER force field to yield the OPLS-UA/AMBER force field for peptides and proteins [57]. In OPLS-AA, bond stretching and angle bending were described by harmonic potentials (Eqs. 20 and 22). The OPLS-UA and OPLS-AA force fields consider the energetic contribution of the torsional motion by a Fourier series truncated after the third term (Eq. 25). The Van der Waals interactions are represented by the LJ 12-6 potential and electrostatics is represented by point charges. The LJ potential is not only used to describe the intermolecular interactions, but also the interactions between different sites of the same molecule that are separated by three (1-4 potential) or

more bonds. The intramolecular 1-4 potential is scaled for both the LJ and Coulombic contributions by an empirical factor. The OPLS-AA force field uses a scaling factor of 1/2 for both potentials, while the OPLS-UA/AMBER force field uses factors of 1/2 and 1/8, respectively. Also, the unlike LJ parameters are defined by the geometric mean for the size and energy parameter, cf. Eq. 11. Different OPLS force field versions were optimized applying different methods. Geometrical parameters, such as for bond stretching and angle bending, were taken from other force fields (AMBER94 [66], CHARMM [91, 95, 140]), fitted to experimental molecular structures or to *ab initio* calculations at the HF/6-31G* level of theory. The rotational terms of the OPLS-UA force field were derived from rotational potentials obtained by molecular mechanics (MM) simulations, while in the most recent versions of the OPLS-AA force field, the torsional potentials were fitted to *ab initio* calculations at the MP2 level of theory with the 6-31G* or even the correlation consistent polarized triple zeta (cc-pVTZ) basis set. The parameterization of the intermolecular interactions was performed to reproduce saturated liquid density and enthalpy of vaporization. In some versions of the OPLS-AA force field [137, 138], the partial charges were fitted to the *ab initio* ESP with the CHELPG [79] procedure. Since the OPLS-UA force field for hydrocarbons was parameterized considering primarily short alkane chains, the deviations to experimental vapor-liquid equilibrium data become more significant for larger chain lengths [141].

4.1.2 TraPPE Force Field

The transferable potential for phase equilibria (TraPPE) was originally developed by devising a united-atom representation for the alkyl segments (TraPPE-UA), however, a TraPPE force field with explicitly considered hydrogens (TraPPE-EH) [119] was also formulated. The TraPPE force field is available for a large number of compound families, including linear and branched alkanes [117, 118], alcohols [114], ethers [120], ketones [120], glycols [120], amines [122], amides [122], tiols [115], aromatics [119, 121], acrylates [116], among others. The TraPPE force field takes the intermolecular interactions into account by the LJ 12-6 potential (Eq. 6) and Coulombic terms (Eq. 14). For the unlike LJ interactions, the standard Lorentz-Berthelot combining rule (Eq. 12) is assumed. The intramolecular interactions covered by this force field are: angle bending on the basis of a harmonic potential (Eq. 22) and torsional motion expressed as a set of cosine series and a harmonic improper dihedral potential (Eq. 27). The bond lengths are fixed, thus bond-stretching is not taken into account. Usually, the intramolecular parameters for angle bending were transferred from the AMBER94 [66] force field and the dihedral parameters were taken from the OPLS-UA force field. The LJ and point charge parameters were fitted to reproduce experimental vapor-liquid coexistence data. The TraPPE force field reproduces the saturated liquid density of linear alkanes with a mean accuracy of approximately 1%, which has to be seen in the light of traditional predictive methods like Lee-Kesler that have an accuracy of 2-3% [9]. The TraPPE force field reproduces vapor pressure, saturated vapor density and critical point with

more significant deviations to the experiment [9]. It does not reproduce the second virial coefficient well and consistently underpredicts the shear viscosity of short chain paraffins [106].

4.1.3 OPPE-AUA4 Force Field

The anisotropic united-atom optimized potential model for phase equilibria (OPPE) force field is an elaboration of the anisotropic united-atom (AUA) force field, initially proposed by Toxvaerd [142, 143] that was further developed by Ungerer and coworkers [130]. This force field is currently available for n-alkanes [130], olefins [59], alcohols [68], polyalcohols [144], amines [123], amides [123], nitriles [127], sulfides [126], thiols [126], ketones [128], aromatic hydrocarbons [124, 129] or polycyclic aromatics [125]. The major novelty of AUA force fields was that the force center is spatially located between the carbon and the hydrogen atoms of the represented molecular group. The intermolecular interactions were described by the LJ 12-6 potential and point charges (Eqs. 6 and 14). The Lorentz-Berthelot combining rule (Eq. 12) was used for the unlike LJ parameters. As in the TraPPE force field, the bond lengths were kept fixed. Angle bending was modeled by a trigonometric potential (Eq. 23) and the torsional potential following Ryckaert and Belleman (Eq. 24). Some angle parameters were taken from the AMBER94 [66] force field and the torsional potential parameters were taken from the OPLS-UA [96] force field. In other cases, molecular geometry and electrostatic charges were determined from *ab initio* calculations. Usually, geometries were optimized with the B3LYP functional and the 6-311G** basis set. The partial charges were parameterized according to the procedure of Lévy and Enescu [145] to reproduce the ESP around the isolated molecule for several representative conformations using RESP [80]. The *ab initio* ESP of the molecules was determined at the MP2 level of theory with a 6-31G* or a 6-311G** basis set. The LJ parameters were optimized to reproduce experimental values of saturated liquid density, enthalpy of vaporization and vapor pressure. The OPPE force field provides a good representation of the vapor pressure and a very accurate representation of the liquid density over a wide temperature range for n-alkanes, branched alkanes and cycloalkanes [56]. The vapor pressure of alkanes is predicted with an average deviation to experimental data of 15%, compared to 30% for the TraPPE force field and 35% for classical prediction methods based on boiling temperature and heat of vaporization [9]. Since transport properties are not well predicted by this force field, Nieto-Draghi et al. [107] proposed a modification of the OPPE model by adjusting the parameters of the torsional potential to reproduce experimental values of reorientation dynamics and shear viscosity.

4.1.4 NERD Force Field

The Nath, Escobedo and de Pablo (NERD) force field [100, 131, 132, 133] was developed to provide accurate predictions of thermodynamic properties. It is currently available for linear [100] and branched alkanes [131, 133] as well as for alkenes [132]. It has a similar functional form as the TraPPE-UA force field, but bond-stretching is included. This interaction and angle bending are represented by harmonic potentials (Eqs. 20 and 22). The torsional potential is of the form of Eq. 25, neglecting cross terms. The LJ 12-6 potential (Eq. 6) is used to describe the intermolecular and intramolecular interactions between sites that are separated by more than three bonds. The LJ parameters were obtained from fits to experimental liquid density and second virial coefficient. Saturated liquid densities from NERD force fields are in good agreement with experimental data. However, the vapor pressure predictions are typically slightly above experimental data at low temperatures and below experimental data at high temperatures [56], while the critical temperature is overestimated, e.g. by 7 K for short-chain alkanes (ethane and pentane) [18].

4.1.5 GIBBS99 Force Field

The GIBBS99 exponential-6 force field [18] is a united atom representation that is available for linear alkanes, cyclohexane or benzene [134]. It differs from the NERD and TraPPE force fields in the description of the Van der Waals interactions: The Buckingham exponential-6 potential (Eq. 7) was used instead of the LJ 12-6 potential. Similarly to the TraPPE force field, bond stretching was neglected, however, the bond length between two methyl groups of the alkane chain was not fixed as in the TraPPE force field, but depends on the molecular groups that form the bond. Angle bending was represented by the harmonic potential (Eq. 22) and the torsional motion by a third order Fourier series (Eq. 25). The force field parameters were fitted to critical properties and saturated densities. The GIBBS99 force field represents the vapor pressure and saturated densities for the alkanes from ethane to n-dodecane with average deviations of around 2%. The experimental vapor pressures for benzene and cyclohexane are reproduced with average errors of 2.6 and 1.7%, respectively [134].

4.1.6 Other Force Fields

Transferable force field families intended for biological applications are sometimes applied in chemical engineering for the simulation of large molecules like polymers. Also, some ionic liquids were parameterized in that framework [105]. Some relevant force fields are: Chemistry at Harvard molecular mechanics (CHARMM) [95, 91, 140], assisted model building with energy refinement (AMBER) [65, 66, 146, 147], Groningen molecular simulation (GROMOS) [148, 149, 150], condensed-phase optimized molecular potentials for atomistic simulation studies (COMPASS) [70],

consistent force field (CFF) [151, 152, 153], among many others. These force fields best reproduce the data for which their parameters were optimized. AMBER, CHARMM and OPLS-AA overestimate the free energy of hydration of protein functional groups [154]. Several works on the comparison of various of these force field families for the simulation of proteins [155, 156, 157, 158, 159], deoxyribonucleic acids [160], peptides [161], carbohydrates [162] or aqueous salt solutions [163] can be found in literature.

Some examples for transferable polarizable force fields are: Drude [83], TraPPE-pol, CHARMM-FQ [164], PIPF [165, 166, 167] and AMOEBA [168]. A review on polarizable force fields can be found e.g. in [45]. Many of the mentioned force fields for biochemical applications as well as the polarizable force fields are being continuously developed, improved and refined. Therefore, numerous versions of each family can be found in the literature.

4.1.7 Force Fields Comparison

Martin [169] compared the AMBER, CHARMM, COMPASS, GROMOS, OPLS-AA and TraPPE force fields with respect to their ability to predict vapor-liquid equilibrium properties and the liquid density of small alkanes and alcohols. He concluded that the force field families performing best for fluid phase simulations are TraPPE and CHARMM. CHARMM better predicts the vapor density, while TraPPE has a higher accuracy for liquid density predictions.

TraPPE and OPPE-UA are, to our opinion, the best transferable force fields developed to date for chemical engineering applications. However, they still have some deficiencies. The capabilities of these force field families are still less explored than group contribution methods like UNIFAC in phenomenological thermodynamics.

4.2 Specific Force Fields

A force field that is carefully parameterized for a specific substance is usually more accurate than a transferable force field. Therefore, when high levels of accuracy are required, specific force fields are preferred. Most of the newer specific force fields developed for engineering applications were parameterized to reproduce experimental data on saturated liquid density and enthalpy of vaporization. The use of *ab initio* calculations gained importance in the last decade and the majority of force field developers nowadays thus makes use of QM calculations to some extent. There are numerous parameterization strategies for the development of such force fields, which depend on the availability of experimental data and the complexity of the chosen functional form. There is an immense number of specific force fields, therefore it is impossible to give a comprehensive overview here. Only a small selection will be discussed in the following to exemplify different parameterization strategies.

The re-parameterization of existing or transferable force fields using a different set of experimental or *ab initio* data as in [170] will not be treated in further detail.

4.2.1 Empirical Force Fields

All transferable force fields discussed in section 4.1 employ point charges to account for the molecular charge distribution, although for a more accurate description of the electrostatics with higher multipole moments may be used. Hasse, Vrabec and co-workers [102, 109] proposed a set of simple united-atom force fields for more than 70 compounds of different classes that describe the intermolecular interactions using two LJ 12-6 sites plus a point dipole or a point quadrupole. The potential model parameters were optimized to experimental critical temperature, saturated liquid density and vapor pressure, thus, no direct information on the multipole moments or the geometry was taken into account. These force fields allow to describe the vapor-liquid equilibria with an average accuracy of 4% for the vapor pressure, 0.5% for the saturated liquid density and 3% for the enthalpy of vaporization throughout the entire temperature range from the triple point to the critical point. Furthermore, the shear viscosity and the thermal conductivity are predicted within 10% accuracy [171, 172]. It can be argued that oversimplified molecular models can be adjusted to a few experimental pure substance properties, but major deficiencies should be visible when applied to mixtures. Recently, all systems for which experimental mixture data was available containing these simple models were studied by molecular simulation [39, 40, 41] using one experimental data point to obtain the adjustable combining rule parameter ξ (Eq. 13). The results of this study were very satisfactory.

4.2.2 Semi-Empirical Force Fields

Fermeglia et al. [173] proposed flexible all-atom force fields for several hydrofluorocarbons to describe vapor-liquid equilibria. They used a more complex expression for the potential energy including intramolecular interactions, i.e. bond stretching (Eq. 20), angle bending (Eq. 23) and torsional motion (Eq. 24). The intermolecular interactions were represented by the LJ 12-6 potential and partial charges (Eqs. 6 and 14). The parameters of the intramolecular terms were determined by geometry optimization and potential energy surface sampling. For this purpose, DFT with the BPW91 functional was employed [173]. The partial charges were obtained from fits to the ESP, while the LJ parameters were optimized to experimental data on liquid density and cohesive energy. These force fields predict the phase behavior with an average error of about 2% for saturated densities in the temperature range from 200 to 380 K.

Hasse, Vrabec and co-workers [86, 174] presented a set of semi-empirical rigid, united-atom force fields for hazardous fluids, such as cyanide, acetonitrile, nitromethane or phosgene. They described the intermolecular interactions with LJ

12-6 sites and point charges, point dipoles or point quadrupoles. The geometric parameters of these force fields, i.e. bond lengths, angles and dihedrals, were determined by *ab initio* calculations at the HF/6-31G level of theory. The electrostatic multipole moments (dipoles and quadrupoles) were obtained by integration over the orbitals from the electron density distribution, using QM at the MP2 level of theory with a 6-31G(d,p) basis set. The LJ parameters and point charge magnitudes were optimized to experimental vapor-liquid equilibrium data. These specific force fields describe vapor-liquid equilibrium properties with a better accuracy than the available transferable force fields [86].

A united-atom force field based on GROMOS96 [148] was proposed by Micaelo et al. [105] for imidazolium-based ionic liquids. They used *ab initio* calculations at the HF/6-31G* level of theory to obtain partial charges based on the single-step RESP method. Bond lengths and bond angles were constrained to reproduce the optimum geometry from QM calculations. The LJ parameters were optimized to experimental values of shear viscosity, self-diffusion coefficient and liquid density. A review on force fields for the simulation of imidazolium-based ionic liquids can be found in [175].

Liu et al. [176] developed force fields for guanidinium-based ionic liquids following the AMBER force field approach. The intramolecular interactions of their force fields include harmonic bond stretching and angle bending, together with torsional motions. The equilibrium bond lengths and bond angles were taken from QM calculations at the HF/6-31+G(d) level. The force constants were adjusted to vibrational frequencies obtained by *ab initio* calculations or from experiment. Single point MP2/6-31+G(d) calculations were taken to parameterize the torsional potential and QM calculations at the B3LYP/6-31+G(d) level to obtain RESP charges. The LJ parameters were transferred from the AMBER99 force field.

4.2.3 *Ab Initio* Force Fields

Hellmann et al. [23, 177, 178] have proposed *ab initio* force fields for several small molecules, such as helium, neon or methane, based on the Tang and Toennies potential (Eq. 9) and Coulombic terms (Eq. 14). With these force fields, gas phase properties like second virial coefficient, shear viscosity, thermal conductivity or self-diffusion coefficient can be predicted extremely accurately. Typically, the generated data are within the experimental uncertainty.

Domański et al. [179] developed a *ab initio* force field for liquid carbon dioxide by fitting the LJ parameters and the Coulombic terms to the potential energy surface calculated with QM at the MP2 level of theory and the 6-31G* basis set. Unfortunately, their model does not reproduce the thermodynamic behavior of the liquid state so that an empirical scaling factor had to be adjusted to experimental data.

Hloucha et al. [24] developed force fields for methanol and acetonitrile from *ab initio* calculations for the prediction of macroscopic properties. These all-atom force fields include LJ 12-6 or modified Buckingham exponential 6 sites plus partial charges. Interaction energies for many hundreds of configurations calculated via

symmetry adapted perturbation theory (SAPT) were employed for the parameterization of the LJ and Buckingham terms. To cover electrostatics, the charges were fitted to the ESP from quadratic configuration interaction with single and double substitution (QCISD) calculations and the augmented correlation-consistent polarized valence double-zeta basis set (aug-cc-pVD). Despite the fact that the force field for acetonitrile yields a reasonable agreement with the experiment for vapor-liquid equilibrium properties, for methanol, the saturated liquid density was strongly underpredicted and the vapor pressure was overpredicted by one order of magnitude. Cabaleiro-Lago and Ríos [20] proposed a similar *ab initio* force field for acetonitrile optimized at the MP2/6-311+G* level of theory. However, their force field gives a poor prediction of the phase behavior [24]. Further examples of *ab initio* force fields can be found e.g. in [69].

5 Molecular Simulation Methods

Given an adequate force field, molecular simulation is in principle capable to yield predictions of thermodynamic properties for a broad range of thermodynamic conditions. To this end, different simulation techniques can be employed, which can be divided in MD and MC. Here, some simulation tools for predicting thermodynamic properties that are important for chemical engineering, i.e. vapor-liquid equilibrium and transport properties, will be addressed briefly.

5.1 Molecular Dynamics

MD is a technique in which the time evolution of the molecular motions is simulated following the laws of classical mechanics. Therefore, the physical variable time must be considered explicitly. In this way, the dynamic evolution of coordinates and moments, i.e. the trajectory of the system, is calculated by numerically solving Newton's equations of motion. This trajectory, together with the associated energies and forces, leads to the static and dynamic thermodynamic properties of the studied system via statistical analysis methods. MD is also a powerful tool to understand dynamic processes at the atomistic level that involve fluids or materials [9].

In MD, a set of second order differential equations is solved by finite difference techniques. This can be done with a variety of integration algorithms, such as Verlet, velocity Verlet, Leap-Frog or Gear predictor-corrector. Although the microcanonical (*NVE*) ensemble is the most natural one for MD simulations, generally the canonic (*NVT*) or the isobaric-isothermal (*NpT*) ensembles are applied. Particularly in chemical engineering, physical properties are needed for specified thermodynamic conditions like temperature or pressure. Several methods exist to control temperature and pressure during simulation, e.g. velocity scaling, Anderson thermostat, Berendsen thermostat, Nosé-Hoover thermostat, Nosé-Hoover chains ther-

mostat or Berendsen barostat. A description of these algorithms can be found e.g. in [11, 180].

A MD simulation yields a significant amount of useful information for chemical engineering applications [11]. E.g., it is employed to study dynamic processes, like diffusion, adsorption or glass transition. A review of MD applications can be found e.g. in [9].

5.2 Monte Carlo

MC is a stochastic method that samples the configuration space of a system with a specified Hamiltonian [181]. In MC simulations, the transition between states or configurations is achieved by a random generation of a new state, evaluating a probabilistic acceptance criterion and accepting or rejecting the perturbation. New configurations are usually generated by displacing, removing or adding individual molecules. The acceptance of new states is performed most commonly according to the Metropolis criterion.

In the production phase of MC simulations, all configuration-dependent properties fluctuate around constant average values that correspond to the thermodynamic equilibrium. Each state is thereby sampled with a frequency proportional to its equilibrium probability density [182]. In the canonical ensemble the probability density ρ_m^{NVT} is given by [181]

$$\rho_m^{NVT} = \frac{\exp(-E_m/(k_B T))}{\sum_{\text{allstates}} \exp(-E_m/(k_B T))}, \quad (28)$$

where k_B is the Boltzmann constant and E_m is the potential energy of a state m .

An advantage of MC is that it can be readily adapted to any ensemble [11]. Therefore, many MC ensembles have been developed for the simulation of specific systems or properties. A wide variety of MC simulation techniques can thus be found in the literature. Reviews and detailed information about MC techniques are presented e.g. in [11, 181, 182, 183, 184, 185].

5.3 Methods for Determining Phase Equilibria

The calculation of vapor-liquid equilibria by molecular simulation is a longstanding and important task. In the last two decades a variety of methods for this purpose have been presented. There are, among others, thermodynamic scaling [186], histogram reweighting [187, 188], Gibbs-Duhem integration [189], NpT plus test particle method [190], grand canonical ensemble [191], grand equilibrium method [192], or the Gibbs ensemble MC method [193]. Here, some of these simulation tools

will be briefly addressed. A throughout discussion of the different approaches can be found e.g. in [181, 182, 194, 195].

The Gibbs ensemble MC method (GEMC) [193] was developed to sample two homogeneous coexisting phases that are in thermodynamic equilibrium, but not in physical contact with each other. The pressure and chemical potential of the phases are equated by allowing the volume and the number of molecules to fluctuate between the phases, while keeping the total volume and total number of molecules constant. This ensemble is widely employed to calculate phase equilibria [18], also in combination with Gibbs-Duhem integration [189, 196]. It is also used to simulate chemical reactions in phase equilibrium [197, 198]. In the literature, some advanced methods related to this ensemble can be found, e.g. the thermodynamic scaling Gibbs ensemble [199].

In the grand canonical (GC) ensemble, a system at constant temperature, volume and chemical potential is considered. The number of molecules is therefore allowed to fluctuate. In such simulations, molecule displacement, insertion and deletion are attempted. From a series of several GCMC simulations, the pressure dependence of the chemical potential in the vapor and in the liquid phase can be obtained. The coexistence condition is then found at the intersection point [181]. The number of molecules is not constant for this ensemble and the coexisting phases are simulated independently. The semigrand canonical ensemble [200, 201] was introduced to overcome the low acceptance probability of molecule insertions and deletions for liquids in the GC ensemble. Furthermore, the GC ensemble can be combined with finite-size scaling methods, e.g. to evaluate the surface tension [202, 203].

Another technique to determine the vapor-liquid equilibrium of pure substances or mixtures, which has some similarities with [190, 204, 205, 206], is the grand equilibrium method [192]. It is a two-step procedure, where the coexisting phases are simulated independently and subsequently. In the first step, one NpT simulation of the liquid phase is performed to determine the chemical potentials μ_i^l and the partial molar volumes v_i^l of all components i . These entropic properties can be determined by Widom's test molecule method [207] or more advanced techniques, such as gradual insertion [208, 209, 210] (see below). On the basis of the chemical potentials and partial molar volumes at a specified pressure p_0 , first order Taylor expansions can be made for the pressure dependence

$$\mu_i^l(T, x, p) \approx \mu_i^{l,\text{id}}(T) + \mu_i^{l,\text{re}}(T, x, p_0) + v_i^l(T, x, p_0) \cdot (p - p_0), \quad (29)$$

where $\mu_i^{l,\text{id}}(T)$ is the solely temperature dependent ideal contribution and the residual chemical potential is $\mu_i^{l,\text{re}}(T, x, p_0)$. Note that $\mu_i^{l,\text{id}}(T)$ does not need to be evaluated for vapor-liquid equilibrium calculations, because it cancels out when Eq. 29 is equated to the corresponding expression for the vapor. In the second step, one pseudo- μVT simulation [192] is performed for the vapor phase on the basis of Eq. 29 that yields the saturated vapor state point of the vapor-liquid equilibrium. This simulation takes place in a pseudo-ensemble in the sense that the specified chemical potentials are not constant, but dependent on the actual pressure in the vapor phase. Thus the vapor simulation rapidly converges to the saturated vapor state

point during equilibration so that effectively the equilibrium chemical potentials are specified via the attained vapor pressure. The grand equilibrium method has been extensively used for the determination of vapor-liquid equilibria of hundreds of systems [40, 41].

Several methods to obtain vapor-liquid equilibria or the Henry's law constant [39] require the accurate calculation of the chemical potential. Widom's test molecule method [207] is the most common approach for that task. Widom's method randomly introduces test molecules of the component for which the chemical potential is evaluated into the simulation volume, to calculate their potential energy ψ_i . The test molecules are instantly removed after the calculation and do not influence the remaining molecules. Widom's method is applicable to MC as well as to MD simulations [56]. In the NVT ensemble, the residual chemical potential μ_i^{re} of component i is calculated by

$$\mu_i^{\text{re}} = -k_B T \ln \langle \exp(-\psi_i / (k_B T)) \rangle. \quad (30)$$

Widom's method has problems dealing with very dense and strongly interacting fluids, because inserted test molecules almost always overlap with "real" molecules, which leads to extremely large values for the potential energy ψ_i . These insertions contribute with little information resulting in poor statistics [56]. Therefore, advanced methods have been proposed in the literature. An example is the gradual insertion method [208, 209, 210], where a fluctuating molecule is introduced into the simulation. The fluctuating molecule undergoes a stepwise transition between non-existence and existence, which allows determining the chemical potential. This method has successfully been applied to vapor-liquid equilibrium calculations of numerous binary and ternary mixtures [40, 41, 174]. Many other methods, such as configurational biased insertion [211] or minimum mapping [212], have been proposed in the literature. A detailed description and comparison thereof can be found e.g. in [213].

The Henry's law constant can be obtained from molecular simulation using several approaches [214, 215]. It is related to the residual chemical potential of the solute i at infinite dilution μ_i^∞ by [216]

$$H_i = \rho k_B T \exp(\mu_i^\infty / (k_B T)), \quad (31)$$

where ρ is the density of the solvent.

5.4 Methods for Determining Transport Properties

Transport properties, such as diffusion coefficients, shear viscosity, thermal or electrical conductivity, can be determined from the time evolution of the autocorrelation function of a particular microscopic flux in a system in equilibrium based on the Green-Kubo formalism [217, 218] or the Einstein equations [219]. Autocorrelation functions give an insight into the dynamics of a fluid and their Fourier transforms

can be related to experimental spectra. The general Green-Kubo expression for an arbitrary transport coefficient γ is given by:

$$\gamma = \frac{1}{G} \int_0^{\infty} dt \langle \dot{\mathbf{A}}(t) \cdot \dot{\mathbf{A}}(0) \rangle, \quad (32)$$

and the general Einstein or square displacement formula can be written as

$$\gamma = \frac{1}{2Gt} \langle [\dot{\mathbf{A}}(t) - \dot{\mathbf{A}}(0)]^2 \rangle. \quad (33)$$

Therein, G is a transport property specific factor, \mathbf{A} the related perturbation and $\dot{\mathbf{A}}$ its time derivative. The brackets $\langle \dots \rangle$ denote the ensemble average. It was shown that Eq. 33 can be derived from Eq. 32, thus both methods are equivalent [220].

In case of the self-diffusion coefficient, $\mathbf{A}(t)$ is the position vector of a given molecule at some time t and $\dot{\mathbf{A}}(t)$ is its center of mass velocity vector. In this way, the self-diffusion coefficient is related to the velocity autocorrelation function. On the other hand, the shear viscosity is associated with the time autocorrelation function of the off-diagonal elements of the stress tensor. The thermal conductivity and the electrical conductivity are related to the autocorrelation functions for the energy and electrical current, respectively.

Beside the Green-Kubo and the Einstein formulations, transport properties can be calculated by non-equilibrium MD (NEMD) methods. These involve an externally imposed field that drives the system out of the equilibrium. Similar to experimental approaches, the transport properties can be extracted from the long-time response to this imposed perturbation. E.g. shear flow and energy flux perturbations yield shear viscosity and thermal conductivity, respectively. Numerous NEMD algorithms can be found in the literature, e.g. the Dolls tensor [221], the Sllod algorithm [222] or the boundary-driven algorithm [223]. A detailed review on several NEMD approaches can be found e.g. in [224].

The NEMD methods are based on the general expression [225]

$$\gamma = \lim_{F_e \rightarrow 0} \lim_{t \rightarrow \infty} \frac{\langle J(t) \rangle}{F_e}, \quad (34)$$

where $\langle J(t) \rangle$ is the steady state average of the thermodynamic flux $J(t)$ perturbed by the external field F_e . Although a methodology for calculating diffusion coefficients with NEMD is available, such methods are predominantly employed to calculate the shear viscosity and the thermal conductivity [226, 227]. NEMD methods are favored when the signal-to-noise ratio is high at long times. There is an extensive on-going discussion on whether or not NEMD methods should generally be preferred over equilibrium MD [11, 225, 228, 229].

5.5 Simulation Tools

There are numerous available open source and commercial molecular simulation codes. Examples for MD codes are: CHARMM [230], DL-POLY [231], GRO-MACS [232], LAMMPS [233], MACSIMUS [234], Moldy [235], *ms2* [236], NAMD [237], Tinker [238] or YASP [239]. Some MC simulation codes are: BIGMAC [240], BOSS [241], GCMC [242], MedeA Gibbs [243], MCCCSTowhee [244] or *ms2* [236]. These software packages have been developed for different applications and show large differences in terms of performance, parallelization paradigm and handling. Most of them use their own input and force field files as well as analysis programs to compute the desired properties from the simulation output. Many simulation tools are in constant development and have an increasing number of active users, thus their supported features are constantly changing.

6 Case Study: Ammonia

Ammonia is one of the most important industrial chemicals. Due to its relevance and its simple symmetric molecular structure, much work has been devoted to the development of a force field that is capable to accurately predict a broad range of its thermodynamic properties. In the following, the capabilities of force fields fitted to QM and vapor-liquid equilibrium data to predict other pure component properties over a wide range of states are addressed.

6.1 Force Fields

Several semi-empirical and empirical force fields have been developed for ammonia [108, 139, 245, 246, 247, 248, 249, 250, 251, 252, 253]. In this work, some rigid, non-polarizable models optimized with different parameterization strategies will be addressed. Jorgensen and Ibrahim [245] used experimental geometric information, i.e. bond lengths and bond angles, together with *ab initio* information to devise a force field based on one LJ 12-6 site and four point charges. They used the STO-3G minimal basis set to calculate the energy of 250 different ammonia dimer configurations. An empirical scaling factor was adopted to account for the polarizability in the liquid phase. Hinchliffe et al. [246] followed a similar parameterization strategy, but employed a Morse potential for repulsion and dispersion. The parameters of the Morse potential and the four point charges were fitted to the dimer energy surface calculated with the 6-31G* basis set for seven different dimer configurations. The geometric parameters were taken from experimental results. Impey and Klein [108] re-parameterized the model by Hinchliffe et al. [246] and replaced the Morse potential with one LJ 12-6 site located at the nitrogen nucleus to describe the dispersive and repulsive interactions. They kept the point charges at the hydrogen nucleus po-

sitions, but displaced the nitrogen partial charge towards the hydrogen atoms. The parameters of this five-site model were optimized to the radial distribution function of liquid ammonia.

Kristóf et al. [252] proposed an empirical force field, fitted to experimental molecular geometry and vapor-liquid equilibrium properties. This force field consists of one LJ 12-6 site plus four partial charges. Recently, Zhang and Siepmann [253] proposed a five-site ammonia force field based on the geometry of the Impey and Klein [108] model. This force field also consists of one LJ 12-6 site and four partial charges, three of them located at the hydrogen positions and one located in a distance of 0.08 Å from the nitrogen nucleus. The LJ parameters, partial charge magnitudes and the position of the displaced nitrogen charge were optimized to vapor-liquid equilibrium data.

Eckl et al. [97] introduced a semi-empirical force field for ammonia also based on one LJ 12-6 site and four partial charges that are located at the nitrogen and hydrogen positions. The geometry was calculated at the self-consistent field HF level of theory with a 6-31G basis set. The resulting geometry ($r_{\text{NH}} = 1.0136$ Å, $\angle_{\text{HNH}} = 105.99^\circ$) is very close to the experimental data ($r_{\text{NH}} = 1.0124$ Å, $\angle_{\text{HNH}} = 106.67^\circ$) [254]. Eckl et al. [97] adjusted the partial charge magnitudes to the results from a single point QM calculation at the MP2 level of theory with the polarizable basis set 6-311G(d,p) using the COSMO [90] method to account for the liquid polarizability. Only the two LJ parameters were adjusted to experimental data on saturated liquid density, vapor pressure and enthalpy of vaporization.

6.2 Vapor-Liquid Equilibria of Ammonia

Both, the GEMC and the grand equilibrium method have been applied to evaluate vapor-liquid equilibrium data for ammonia. Kristóf et al. [252] calculated the vapor pressure and saturated densities using the force field by Impey and Klein [108] and found systematic deviations from experimental data, cf. Figure 3. Therefore, they proposed a new ammonia force field that was optimized to vapor-liquid equilibria [252], achieving a better accuracy. Simulated saturated densities and enthalpies based on this force field agree with the experimental data within 1 and 3%, respectively. However, it shows a mean deviation of 13% from experimental vapor pressure data and the critical temperature is underestimated by 2.4% [97]. A further improvement was achieved by the model from Eckl et al. [97] with mean deviations from the critical temperature, saturated liquid density, vapor pressure and enthalpy of vaporization of 0.8, 0.7, 1.6 and 2.7 %, respectively. The recently introduced force field by Zhang and Siepmann [253], reproduces the saturated liquid densities up to 375 K with a similar accuracy as the model of Eckl et al. [97]. This force field predicts the critical density, critical pressure and normal boiling point with deviations of 0.9, 2 and 0.5%, respectively.

Figures 3 and 4 show the saturated densities and the vapor pressure on the basis of the force fields by Impey and Klein [108], Kristóf et al. [252], Zhang and Siep-

mann [253] and Eckl et al. [97] for the whole temperature range from triple point to critical point together with a reference equation of state [255] for comparison.

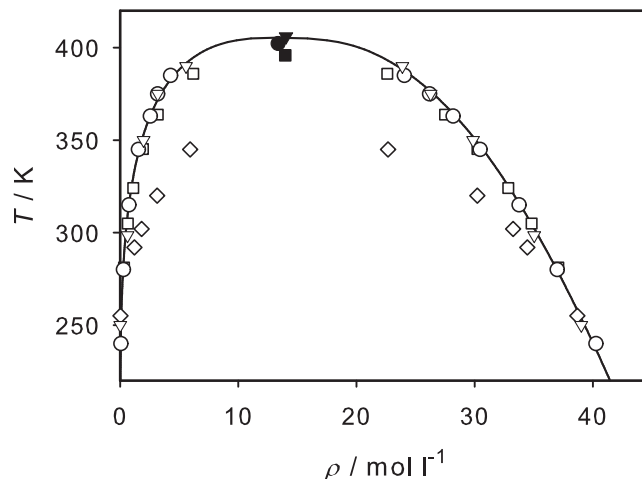


Fig. 3 Saturated densities of ammonia on the basis of different force fields by Impey and Klein (\diamond) [108], Kristóf et al. (\square) [252], Eckl et al. (\circ) [97] as well as Zhang and Siepmann (∇) [253]. The simulation results are compared with a reference equation of state (—) [255]. The calculated critical points (full symbols) are also shown.

6.3 Properties of the Homogeneous State

As discussed in section 2, force fields should not only be able to represent the thermodynamic properties that were used for their parameterization, but should also be capable to predict other properties at different thermodynamic conditions. The force field for ammonia by Eckl et al. [97] is an example of such a force field.

Eckl et al. [97] predicted the density and the enthalpy of liquid, gaseous and supercritical ammonia at 70 different state points, covering a wide range of states for temperatures up to 700 K and pressures up to 700 MPa. They found typical deviations from experimental data below 3 and 5% for the density and the residual enthalpy, respectively. Figure 5 shows, exemplary, the density results on the basis of this force field compared with a reference equation of state [255].

This model was extensively tested with respect to its ability to yield transport properties. E.g., the self-diffusion coefficient was predicted in the temperature range from 203 to 473 K for pressures between 10 to 200 MPa with a mean deviation of 15% over the whole range of studied conditions. As an example, Figure 6 shows

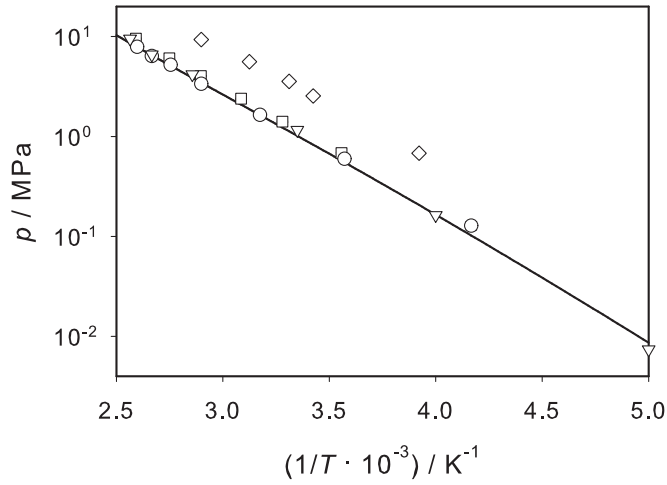


Fig. 4 Saturated vapor pressure of ammonia on the basis of different force fields by Impey and Klein (\diamond) [108], Kristóf et al. (\square) [252], Eckl et al. (\circ) [97] as well as Zhang and Siepmann (∇) [253]. The simulation results are compared with a reference equation of state ($-$) [255].

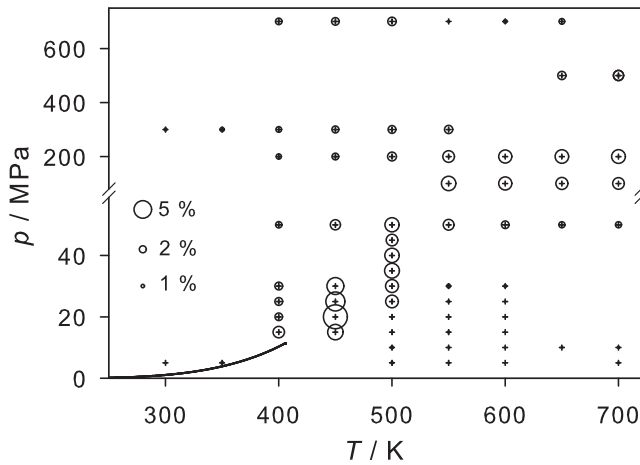


Fig. 5 Relative deviations of the density of ammonia as predicted from the force field by Eckl et al. (+) [97] from a reference EOS [255]. The size of the bubbles denotes the relative deviations as indicated in the plot. The solid line is the vapor pressure curve.

the temperature dependence of the self-diffusion coefficient at 10 and 200 MPa in comparison to experimental data [256].

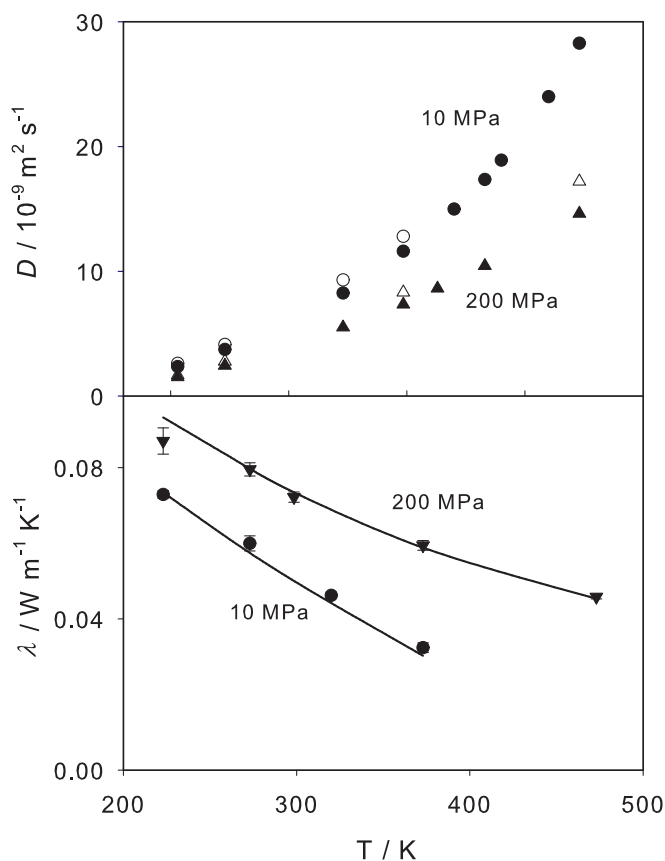


Fig. 6 Temperature dependence of the self-diffusion coefficient (top) and thermal conductivity (bottom) of liquid ammonia on the basis of the force field by Eckl et al. [97]. Simulation results at 10 MPa (●) and 200 MPa (▲) are compared to experimental data (open symbols) [256] and to a correlation of experimental data (–) [257].

The thermal conductivity and the shear viscosity of ammonia were also predicted with a good accuracy on the basis of the force field by Eckl et al. [97] in the same temperature and pressure range. The predictions of the thermal conductivity and the shear viscosity deviate on average by 3 and 14%, respectively from the experimental data.

7 Case Study: Binary Mixtures Containing CO₂

CO₂ is an important substance which is present in many processes in the chemical industry. In the following, a case study on the prediction of the Henry's law constant CO₂ in ethanol and the vapor-liquid equilibrium of the binary mixture CO₂ + C₂H₆ is discussed. The aim is to explore the capabilities of force fields to predict the temperature dependence of the gas solubility and to predict azeotropic behavior.

7.1 Force Fields

The Van der Waals interactions of the force fields for CO₂ and C₂H₆ were described by two LJ 12-6 sites and one point quadrupole, cf. Eq. 16. Both force fields were empirically parameterized to experimental critical temperatures, saturated liquid densities and vapor pressures by means of a non-linear optimization algorithm. For both pure substances, the vapor-liquid equilibrium properties from simulation deviate by less than 1% from the experimental values of saturated liquid density data and less than 3% from the experimental values of vapor pressure and enthalpy of vaporization data.

The force field for ethanol [258] consists of three LJ 12-6 sites plus three point charges and was parameterized to *ab initio* and experimental data. The nucleus positions of all ethanol atoms were computed by QM at the HF level of theory with a 6-31G basis set. This force field is also based on the anisotropic approach of Ungerer et al. [130]. The LJ parameters and the anisotropic offset were fitted to the experimental values of saturated liquid density, vapor pressure and enthalpy of vaporization. The simulation results from this ethanol force field deviate on average from the experimental values of vapor pressure, saturated liquid density and heat of vaporization by 3.7, 0.3 and 0.9%, respectively.

7.2 Henry's Law Constant of CO₂ in Ethanol

Schnabel et al. [258] calculated the Henry's law constant of CO₂ in ethanol. They evaluated the chemical potential with Widom's test molecule method [207], cf. Eq. 30. In this approach by simulating the pure solvent, the mole fraction of the solute in the solvent is exactly zero, as required for infinite dilution, because the test molecules are instantly removed after the potential energy calculation.

The results from Schnabel et al. [258] are in excellent agreement with the experimental data, cf. Figure 7. It has been shown for over one hundred other mixtures [39, 258] that the Henry's law constant can reliably and accurately be obtained by molecular simulation using relatively simple force fields when the unlike LJ interaction is adjusted to a single binary data point from experiment.

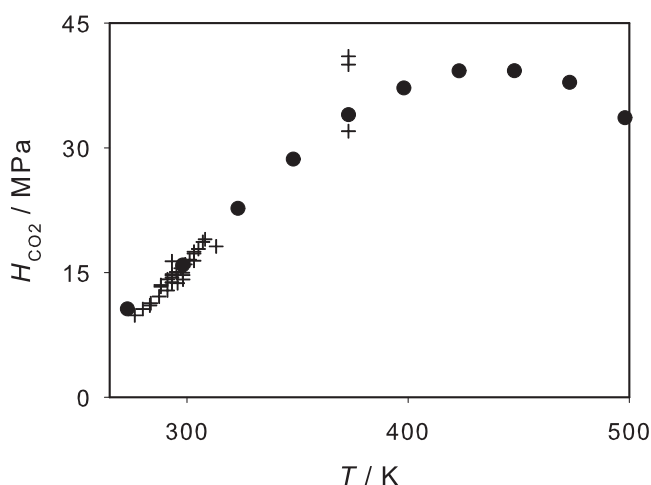


Fig. 7 Henry's law constant of CO₂ in ethanol. The simulation results by Schnabel et al. (●) [258] are compared with experimental data (+) [259, 260, 261, 262, 263, 264, 265].

7.3 Vapor-Liquid Equilibria of the Mixture CO₂ + C₂H₆

Particularly when polar groups are present in liquid mixtures, azeotropes are often formed. For the design of separation processes like distillation, the knowledge of the azeotropic composition at different thermodynamic conditions is of critical importance. In this context, molecular simulation offers a powerful route to predict azeotropic behavior in mixtures. The prediction of the vapor-liquid equilibrium of the mixture CO₂ + C₂H₆ is presented here as an example.

Vrabec et al. [41] predicted the vapor-liquid equilibrium of the mixture CO₂ + C₂H₆ for three different isotherms. The azeotropic behavior of this mixture was predicted using the Lorentz-Berthelot combining rule (Eq. 12), i.e. relying exclusively on pure substance models without considering any experimental binary data. The quality of the predicted data is clearly superior to the Peng-Robinson equation of state with the binary interaction coefficient $k_{ij} = 0$, which shows no azeotrope, cf. Figure 8. As discussed in section 2.1.2, for simulations of binary mixtures unlike LJ parameters are needed. In many cases the Lorentz-Berthelot combining rule (Eq. 12) is too crude to obtain accurate results [34]. Therefore, the modified version of the Lorentz-Berthelot rule (Eq. 13) was preferred. When the binary parameter ξ is adjusted to one experimental binary data point, the simulation results are in excellent agreement with experimental data, cf. Figure 8. The Peng-Robinson EOS, being a workhorse in industrial applications, also shows very good agreement with the experiment when k_{ij} is adjusted.

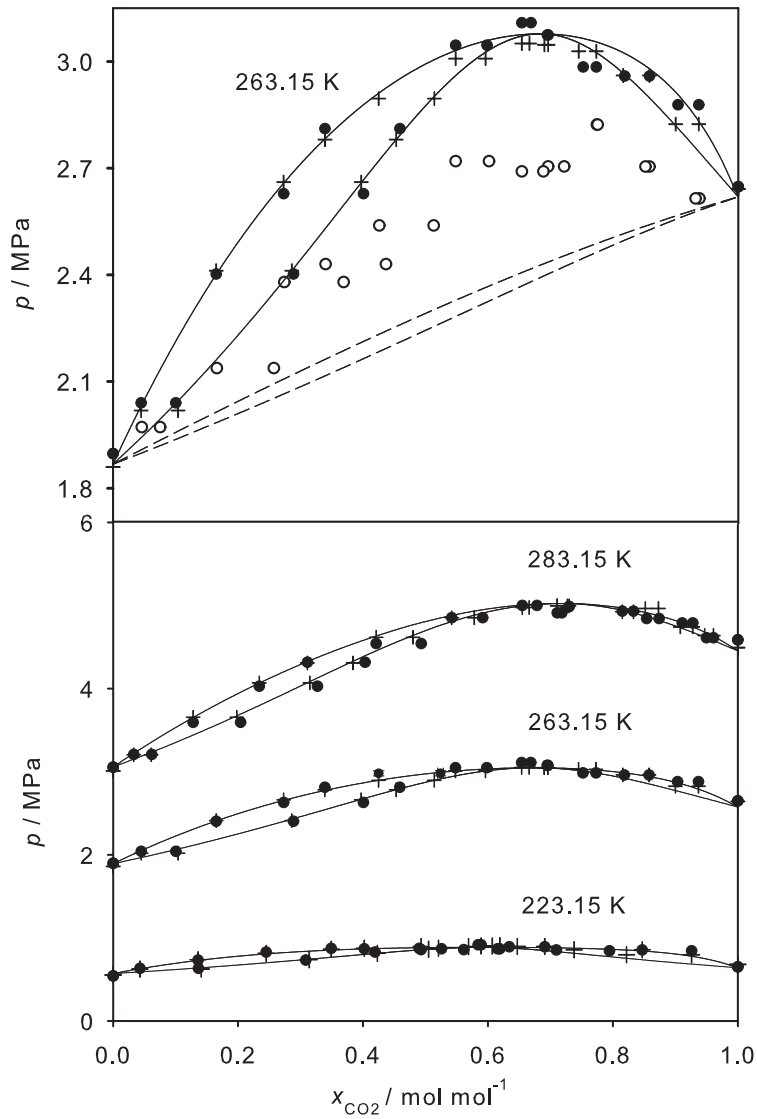


Fig. 8 Vapor-liquid equilibria of the mixture $\text{CO}_2 + \text{C}_2\text{H}_6$. The upper Figure shows a magnified view of the simulation results at 263.15 K by Vrabec et al. [41] with $\xi = 1$ (\circ) and $\xi = 0.954$ (\bullet) compared with experimental data (+) and the Peng-Robinson equation of state with $k_{ij} = 0$ (---) and $k_{ij} = 0.132$ (-). The Figure at the bottom shows the simulation results by Vrabec et al. [41] for 223.15 K, 263.15 K and 283.15 K with $\xi = 0.954$ (\bullet) and the Peng-Robinson EOS with $k_{ij} = 0.132$ (-) compared with experimental data (+) [266].

8 Concluding Remarks

With the ongoing increase of computer performance, molecular modeling and simulation is gaining importance as a tool for predicting the thermodynamic properties for a wide variety of fluids in the chemical industry. One of the major issues of molecular simulation is the development of adequate force fields that are simple enough to be computationally efficient, but complex enough to consider the relevant inter- and intramolecular interactions. There are different approaches to force field development and parameterization. Parameters for molecular force fields can be determined both bottom-up from quantum chemistry and top-down from experimental data.

Transferable force fields have the benefit that they are ready to use and do not need to be fitted for each component individually, however, at the expense of prediction accuracy. On the other hand, specific force fields, parameterized for a single molecule, are time-intensive in the development and require experimental and/or QM data for optimization. Their main advantage is that they can yield excellent accuracies. The advances of the QM methods in the recent years allow for the construction of force fields based on high quality *ab initio* data, i.e. nowadays force fields can be constructed even for new fluids whose properties have been poorly measured or not measured at all. Therefore, molecular modeling and simulation based on classical force fields is a promising alternative route, which in many cases complements the well established methods, like classical equations of state or G^E models.

Acknowledgments

The presented research was conducted under the auspices of the Boltzmann-Zuse Society of Computational Molecular Engineering (BZS). The simulations were performed on the national super computer NEC SX-8 at the High Performance Computing Center Stuttgart (HLRS) under the grant MMHBF and on the HP X6000 super computer at the Steinbuch Center for Computing, Karlsruhe under the grant LAMO. Furthermore, the authors are grateful to Ekaterina Elts and Gabor Rutkai for suggestions on improving the manuscript.

References

1. Hendriks E, Kontogeorgis GM, Dohrn R et al (2010) Industrial Requirements for Thermodynamics and Transport Properties. *Ind Eng Chem Res* 49:11131–11141
2. Dohrn R, Pfohl O (2002) Thermo-physical properties - Industrial directions. *Fluid Phase Equilib* 194–197:15–29
3. Gupta S, Olson JD (2003) Industrial Needs in Physical Properties. *Ind Eng Chem Res* 42:6359–6374

4. Rhodes CL (1996) The process simulation revolution: Thermophysical property needs and concerns. *J Chem Eng Data* 41:947–950
5. Sandler SI (1994) Thermophysical Properties: What Have We Learned Recently, and What Do We Still Need to Know?. *Int J Thermophys* 15:1013–1035
6. Zeck S, Wolf D (1993) Requirements of thermodynamic data in the chemical industry. *Fluid Phase Equilib* 82:27–38
7. Poling BE, Prausnitz JM, O’Connell JP (2000) *The Properties of Gases and Liquids*, 5th edn. McGraw Hill, New York
8. Gubbins KE, Quirke N (1996) Introduction to Molecular Simulation and Industrial Applications: Methods, Examples and Prospects. In: Gubbins KE, Quirke N (eds) *Molecular Simulations and Industrial Applications*. Gordon and Breach Science Publishers, Amsterdam
9. Maginn EJ, Elliot JR (2010) Historical Perspective and Current Outlook for Molecular Dynamics as a Chemical Engineering Tool. *Ind Eng Chem Res* 49:3059–3078
10. Friesner RA (2005) *Ab initio* quantum chemistry: Methodology and applications. *Proc Nat Acad Sc* 102:6648–6653
11. Allen MP, Tildesley DJ (1997) *Computer Simulation of Liquids*. Clarendon Press, Oxford
12. Burkert U, Allinger NL (1982) *Molecular Mechanics*, ACS Monograph 177. American Chemical Society, Washington D.C.
13. Stone AJ (1996) *The Theory of Intermolecular Forces*. Clarendon Press, Oxford
14. Mie G (1903) Zur kinetischen Theorie der einatomigen Körper. *Ann Phys* 11:657–697
15. Horsch M, Vrabec J, Hasse H (2008) Modification of the classical nucleation theory based on molecular simulation data for surface tension, critical nucleus size, and nucleation rate. *Phys Rev E* 78:011603
16. Horsch M, Vrabec J (2009) Steady-state simulation of homogeneous vapor-liquid nucleation “by the intervention of intelligent beings”. In: Smolík J, O’Dowd CD (eds) *Nucleation and Atmospheric Aerosols*. University of Prague, Prague.
17. Kihara T (1951) The Second Virial Coefficient of Non-Spherical Molecules. *J Phys Soc Jpn* 6:289–296
18. Errington JR, Panagiotopoulos AZ (1999) A New Intermolecular Potential Model for the n-Alkane Homologous Series. *J Phys Chem B* 103:6314–6322
19. Leach AR (2001) *Molecular Modelling Principles and Applications*, 2nd edn. Pearson Education, Edinburgh
20. Cabaleiro-Lago EM, Ríos MA (1997) A Potential Function for Intermolecular Interaction in the Acetonitrile Dimer Constructed from Ab Initio Data. *J Phys Chem A* 101:8327–8334
21. Eggenberger R, Gerber S, Huber H et al (1994) A new *ab initio* potential for the neon dimer and its application in molecular dynamics simulations of the condensed phase. *Mol Phys* 82:689–699
22. Grochola G, Russo S, Snook I (1998) An *ab initio* pair potential for Ne₂ and the equilibrium properties of neon. *Mol Phys* 95:471–475
23. Hellmann R, Bich E, Vogel E (2007) *Ab initio* potential energy curve for the helium atom pair and thermophysical properties of dilute helium gas. I. Helium-helium interatomic potential. *Mol Phys* 105:3013–3023
24. Hloucha M, Sum AK, Sandler SI (2000) Computer simulation of acetonitrile and methanol with *ab initio*-based pair potentials. *J Chem Phys* 113:5401–5406
25. Tang KT, Toennies JP (1980) An improved simple model for the Van der Waals potential based on universal damping functions for the dispersion coefficients. *J Chem Phys* 80:3726–3741
26. Al-Matar AK, Rockstraw D (2004) A generating equation for mixing rules and two new mixing rules for interatomic potential energy parameters. *J Comput Chem* 25:660–668
27. Fender BEF, Halsey GD (1962) Second Virial Coefficients of Argon, Krypton, and Argon-Krypton Mixtures at Low Temperatures. *J Chem Phys* 36:1881–1888
28. Halgren TA (1992) The representation of Van der Waals (vdW) interactions in molecular mechanics force fields: potential form, combination rules, and vdW parameters. *J Am Chem Soc* 114:7827–7843

29. Kong CL (1973) Combining rules for intermolecular potential parameters. II. Rules for the Lennard-Jones (12-6) potential and the Morse potential. *J Chem Phys* 59:2464–2467
30. Sikora PT (1970) Combining rules for spherically symmetric intermolecular potentials. *J Phys B* 3:1475–1482
31. Waldman M, Hagler AT (1993) New combining rules for rare-gas Van der Waals parameters. *J Comput Chem* 14:1077–1084
32. Peña MD, Pando C, Renuncio JAR (1982) Combination rules for intermolecular potential parameters. I. Rules based on approximations for the long-range dispersion energy. *J Chem Phys* 76:325–332
33. Peña MD, Pando C, Renuncio JAR (1982) Combination rules for intermolecular potential parameters. II. Rules based on approximations for the long-range dispersion energy and an atomic distortion model for the repulsive interactions. *J Chem Phys* 76:333–339
34. Schnabel T, Vrabec J, Hasse H (2007) Unlike Lennard-Jones Parameters for Vapor-Liquid Equilibria. *J Mol Liq* 135:170–178
35. Lorentz HA (1881) Über die Anwendung des Satzes vom Virial in der kinetischen Theorie der Gase. *Ann Phys* 12:127–136
36. Berthelot D (1889) Sur le Mélange des Gaz. *Comptes Rendus de l'Académie des Sciences Paris* 126:1703–1706
37. Delhommelle J, Millié P (2001) Inadequacy of the Lorentz-Berthelot combining rules for accurate predictions of equilibrium properties by molecular simulation. *Mol Phys* 99:619–625
38. Ungerer P, Wender A, Demoulin G et al (2004) Application of Gibbs Ensemble and NPT Monte Carlo Simulation to the Development of Improved Processes for H₂S-rich Gases. *Mol Simul* 30:631–648
39. Huang YL, Miroschnichenko S, Hasse H et al (2009) Henry's law constant from molecular simulation: a systematic study of 95 systems. *Int J Thermophys* 30:1791–1810
40. Huang YL, Vrabec J, Hasse H (2009) Prediction of ternary vapor-liquid equilibria for 33 systems by molecular simulation. *Fluid Phase Equilib* 287:62–69
41. Vrabec J, Huang YL, Hasse H (2009) Molecular models for 267 binary mixtures validated by vapor-liquid equilibria: a systematic approach. *Fluid Phase Equilib* 279:120–135
42. Stone AJ (2008) Intermolecular Potentials. *Science* 321:787–789
43. Murthy CS, Singer K, Klein ML et al (1983) Electrostatic interactions in molecular crystals. Lattice dynamics of solid nitrogen and carbon dioxide. *Mol Phys* 50:531–541
44. Hirschfelder JO, Curtiss CF, Bird RB (1954) *Molecular Theory of Gases and Liquids*. John Wiley & Sons, New York
45. Halgren TA, Damm W (2001) Polarizable force fields. *Curr Opin Struct Biol* 11:236–242
46. Rick SW, Stuart SJ (2002) Potentials and algorithms for incorporating polarizability in computer simulations. In: Lipowitz DB, Boyd DB (eds) *Review in Computational Chemistry*. Wiley-VCH, New York
47. Yu H, van Gunsteren WF (2005) Accounting for polarization in molecular simulation. *Comput Phys Commun* 172:69–85
48. Dang LX, Rice JE, Caldwell J et al (1991) Ion solvation in polarizable water: molecular dynamics simulations. *J Am Chem Soc* 113:2481–2486
49. Rick SW, Stuart SJ, Berne BJ (1994) Dynamical fluctuating charge force fields: Application to liquid water. *J Chem Phys* 101:6141–6157
50. Rigby M, Smith EB, Wakeham WA et al (1986) *The forces between molecules*. Clarendon Press, Oxford
51. Simons G, Parr RG, Finlan JM (1973) New alternative to the Dunham potential for diatomic molecules. *J Chem Phys* 59:3229–3234
52. Morse PM (1929) Diatomic molecules according to the wave mechanics. II. Vibrational levels. *Phys Rev* 34:57–64
53. Hünenberger PH, van Gunsteren WF (1997) Empirical classical interaction functions for molecular simulation. In: van Gunsteren WF, Weiner PK, Wilkinson AJ (eds) *Computer Simulation of Biomolecular Systems: Theoretical and Experimental Applications*. Kluwer Academic Publishers, Dordrecht

54. van der Ploeg P, Berendsen HJC (1982) Molecular dynamics simulation of a bilayer membrane. *J Chem Phys* 76:3271–3276
55. Ryckaert JP, Bellemans A (1975) Molecular dynamics of liquid n-butane near its boiling point. *Chem Phys Lett* 30:123–125
56. Economou IG (2004) Molecular simulation of phase equilibria for industrial applications. In: Kontogeorgis GM, Gani R (eds) *Computer Aided Property Estimation for Process and Product Design*. Elsevier, Amsterdam
57. Jorgensen WL, Maxwell DS, Tirado-Rives J (1996) Development of the OPLS All-Atom Force Field on Conformational Energetics and Properties of Organic Liquids. *J Am Chem Soc* 118:11225–11236
58. Foloppe N, MacKerell AD (2000) All-atom empirical force field for nucleic acids: Parameter optimization based on small molecule and condensed phase macromolecular target data. *J Comput Chem* 21:86–104
59. Bourasseau E, Haboudou M, Boutin A et al (2003) New optimization method for intermolecular potentials: Optimization of a new anisotropic united atoms potential for olefins. Prediction of equilibrium properties. *J Chem Phys* 118:3020–3034
60. Faller R, Schmitz H, Biermann O et al (1999) Automatic Parameterization of Force Fields for Liquids by Simplex Optimization. *J Comput Chem* 20:1009–1017
61. Hülsmann M, Köddermann T, Vrabec J et al (2010) GROW: A Gradient-based Optimization Workflow for the Automated Development of Molecular Models. *Comput Phys Commun* 181:499–513
62. Njo SL, van Gunsteren WF, Müller-Plathe F (1995) Determination of force field parameters for molecular simulation by molecular simulation: An application of the weak-coupling method. *J Chem Phys* 102:6199–6207
63. Waldher B, Kuta J, Chen S et al (2010) ForceFit: A Code to fit Classical Force Fields to Quantum Mechanical Potential Energy Surfaces. *J Comput Chem* 31:2307–2316
64. Wang J, Kollman PA (2001) Automatic parameterization of force field by systematic search and genetic algorithms. *J Comput Chem* 22:1219–1228
65. Wang J, Wolf RM, Caldwell JW et al (2004) Development and Testing of a General Amber Force Field. *J Comput Chem* 25:1157–1174
66. Cornell WD, Cieplak P, Bayly CI et al (1995) A Second Generation Force Field for the Simulation of Proteins, Nucleic Acids, and Organic Molecules. *J Am Chem Soc* 117:5179–5197
67. Kaminski G, Friesner RA, Tirado-Rives J et al (2001) Evaluation and Reparametrization of the OPLS-AA Force Field for Proteins via Comparison with Accurate Quantum Chemical Calculations on Peptides. *J Phys Chem B* 105:6474–6487
68. Pérez-Pellitero J, Bourasseau E, Demachy I et al (2008) Anisotropic United-Atoms (AUA) Potential for Alcohols. *J Phys Chem B* 112:9853–9863
69. Sandler SI, Castier M (2007) Computational quantum mechanics: An underutilized tool in thermodynamics. *Pure Appl Chem* 79:1345–1359
70. Sun H (1998) COMPASS: An ab Initio Force-Field Optimized for Condensed-Phase Applications. Overview with Details on Alkane and Benzene Compounds. *J Phys Chem B* 102:7338–7364
71. Löwdin, P (1970) On the nonorthogonality problem. *Adv Quantum Chem* 5:185–199
72. Mulliken RS (1962) Criteria for the Construction of Good Self-Consistent-Field Molecular Orbital Wave Functions, and the Significance of LCAOMO Population Analysis. *J Chem Phys* 36:3428–3440
73. Li J, Zhu T, Cramer CT et al (1998) New Class IV Charge Model for Extracting Accurate Partial Charges from Wave Functions. *J Phys Chem A* 102:1820–1831
74. Reed AE, Weinstock RB, Weinhold FA (1985) Natural population analysis. *J Chem Phys* 83:735–747
75. Bader RFW (1985) *Atoms in Molecules. A Quantum Theory*. Clarendon Press, Oxford
76. Wiberg KB, Rablen PR (1993) Comparison of atomic charges derived via different procedures. *J Comput Chem* 14:1504–1518

77. Mobley DL, Dumont E, Chodera JD (2007) Comparison of charge models for fixed-charge force fields: Small molecule hydration free energies in explicit solvent. *J Phys Chem B* 111:2242–2254
78. Chirlian LE, Francel MM (1987) Atomic charges derived from electrostatic potentials: A detailed study. *J Comput Chem* 8:894–905
79. Breneman CM, Wiberg KB (1990) Determining atom-centered monopoles from molecular electrostatic potentials. The need for high sampling density in formamide conformational analysis. *J Comput Chem* 11:361–373
80. Bayly CI, Cieplak P, Cornell W et al (1993) A well-behaved electrostatic potential based method using charge restraints for deriving atomic charges: the RESP model. *J Phys Chem* 97:10269–10280
81. Stouch TR, Williams DE (1992) Conformational dependence of electrostatic potential derived charges of a lipid headgroup: Glycerolphosphorylcholine. *J Comput Chem* 13:622–632
82. Sigfridsson E, Ryde U (1998) Comparison of methods for deriving atomic charges from the electrostatic potential and moments. *J Comput Chem* 19:377–395
83. Anisimov V, Vorobyov IV, Roux B et al (2007) Polarizable empirical force field for the primary and secondary alcohol series based on the classical Drude model. *J Chem Theory Comput* 3:1927–1946
84. Stone AJ (2005) Distributed Multipole Analysis: Stability for Large Basis Sets. *J Chem Theory Comput* 1:1128–1132
85. Joubert L, Popelier PLA (2002) Improved Convergence of the Atoms in Molecules Multipole Expansion of Electrostatic Interaction. *Mol Phys* 100:3357–3365
86. Eckl B, Vrabec J, Hasse H (2008) Set of molecular models based on quantum mechanical ab initio calculations and thermodynamic data. *J Phys Chem B* 112:12710–12721
87. Tomasi J, Mennucci B, Cammi R (2005) Quantum Mechanical Continuum Solvation Models. *Chem Rev* 105:2999–3093
88. Wong MA, Frisch MJ, Wiberg KB (1991) Solvent effects 1. The mediation of electrostatic effects by solvents. *J Am Chem Soc* 113:4776–4782
89. Wong MA, Frisch MJ, Wiberg KB (1992) Solvent effects 2. Medium effect on the structure, energy, charge density, and vibrational frequencies of sulfamic acid. *J Am Chem Soc* 114:523–529
90. Klamt A (1995) Conductor-like Screening Model for Real Solvents: A New Approach to the Quantitative Calculation of Solvation Phenomena. *J Phys Chem* 99:2224–2235
91. MacKerell AD, Bashford D, Bellott M et al (1998) All-Atom Empirical Potential for Molecular Modeling and Dynamics Studies of Proteins. *J Phys Chem B* 102:3586–3616
92. Kony D, Damm W, Stoll S et al (2002) An Improved OPLS-AA Force Field for Carbohydrates. *J Comput Chem* 23:1416–1429
93. Koch W, Holthausen MC (2001) *A Chemist's Guide to Density Functional Theory*, 2nd edn. Wiley & Sons, New York
94. Lee C, Yang W, Parr RG (1988) Development of the Colle-Salvetti correlation-energy formula into a functional of the electron density. *Phys Rev B* 37:785–789
95. Hatcher A, Guvench O, MacKerell AD (2009) CHARMM Additive All-Atom Force Field for Acyclic Polyalcohols, Acyclic Carbohydrates and Inositol. *J Chem Theory Comput* 5:1315–1327
96. Jorgensen WL, Madura JD, Swenson CJ (1984) Optimized Intermolecular Potential Functions for Liquid Hydrocarbons. *J Am Chem Soc* 106:6638–6646
97. Eckl B, Vrabec J, Hasse H (2008) An optimized molecular model for ammonia. *Mol Phys* 106:1039–1046
98. Schnabel T, Srivastava A, Vrabec J et al (2008) Hydrogen Bonding of Methanol in Supercritical CO₂: Comparison between ¹H-NMR Spectroscopic Data and Molecular Simulation Results. *J Phys Chem B* 111:9871–9878
99. Schnabel T, Vrabec J, Hasse H (2008) Molecular Simulation Study of Hydrogen Bonding Mixtures and New Molecular Models for Mono- and Dimethylamine. *Fluid Phase Equilib* 263:144–159

100. Nath SK, Escobedo FA, de Pablo JJ (1998) On the simulation of vapor-liquid equilibria for alkanes. *J Chem Phys* 108:9905–9911
101. Ponceña A, Rubio AM, Freire JJ (1997) Determination of the potential parameters of a site model from calculations of second virial coefficients of linear and branched alkanes. *Mol Phys* 91:189–201
102. Vrabec J, Stoll J, Hasse H (2001) A set of molecular models for symmetric quadrupolar fluids. *J Phys Chem B* 105:12126–12133
103. Kaminski G, Duffy EM, Matsui T et al (1994) Free Energies of Hydration and Pure Liquid Properties of Hydrocarbons from the OPLS All-Atom Model. *J Phys Chem* 98:13077–13082
104. Fiorini M, Burger K, Mark A et al (2000) A New 2,2,2-Trifluoroethanol Model for Molecular Dynamics Simulations. *J Phys Chem B* 104:12347–12354
105. Micaelo NM, Baptista AM, Soares CM (2006) Parametrization of 1-Butyl-3-methylimidazolium Hexafluorophosphate/Nitrate Ionic Liquid for the GROMOS Force Field. *J Phys Chem B* 110:14444–14451
106. Gordon P (2006) Development of intermolecular potentials for predicting transport properties of hydrocarbons. *J Chem Phys* 125:014504
107. Nieto-Draghi C, Ungerer P, Rousseau B (2006) Optimization of the anisotropic united atoms intermolecular potential for n-alkanes: Improvement of transport properties. *J Chem Phys* 125:044517
108. Impey RW, Klein ML (1984) A simple intermolecular potential for liquid ammonia. *Chem Phys Lett* 104:579–582
109. Stoll J, Vrabec J, Hasse H (2003) A set of molecular models for carbon monoxide and halogenated hydrocarbons. *J Chem Phys* 119:11396–11407
110. Jorgensen WL, Swenson CJ (1985) Optimized Intermolecular Potential Functions for Amides and Peptides. Structure and Properties of Liquid Amides. *J Am Chem Soc* 107:569–578
111. Jorgensen WL (1986) Optimized Intermolecular Potential Functions for Liquid Alcohols. *J Phys Chem* 90:1276–1284
112. Jorgensen WL, Tirado-Rives J (1988) The OPLS Force Field for Proteins. Energy Minimizations for Crystals of Cyclic Peptides and Crambin. *J Am Chem Soc* 110:1657–1666
113. Chen B, Siepmann JI (1999) Transferable potentials for phase equilibria. 3. Explicit-hydrogen description of n-alkanes. *J Phys Chem B* 103:5370–5379
114. Chen B, Potoff JJ, Siepmann JI (2001) Monte Carlo Calculations for Alcohols and Their Mixtures with Alkanes. Transferable Potentials for Phase Equilibria. 5. United-Atom Description of Primary, Secondary, and Tertiary Alcohols. *J Phys Chem B* 105:3093–3104
115. Lubna N, Kamath G, Potoff JJ et al (2005) Transferable potentials for phase equilibria. 8. United-atom description for thiols, sulfides, disulfides, and thiophene. *J Phys Chem B* 109:24100–24107
116. Maerzke KA, Schultz NE, Ross RB et al (2009) TraPPE-UA Force Field for Acrylates and Monte Carlo Simulations for Their Mixtures with Alkanes and Alcohols. *J Phys Chem B* 113:6415–6425
117. Martin MG, Siepmann JI (1998) Transferable potentials for phase equilibria. 1. United-atom description of n-alkanes. *J Phys Chem B* 102:2569–2577
118. Martin MG, Siepmann JI (1999) Novel configurational-bias Monte Carlo method for branched molecules. Transferable potentials for phase equilibria. 2. United-atom description of branched alkanes. *J Phys Chem B* 103:4508–4517
119. Rai N, Siepmann JI (2007) Transferable potentials for phase equilibria. 9. Explicit-hydrogen description of benzene and 5-membered and 6-membered heterocyclic aromatic compounds. *J Phys Chem B* 111:10790–10799
120. Stubbs JM, Potoff JJ, Siepmann JI (2004) Transferable potentials for phase equilibria. 6. United-atom description for ethers, glycols, ketones and aldehydes. *J Phys Chem B* 108:17596–17605
121. Wick CD, Martin MG, Siepmann JI (2000) Transferable Potentials for Phase Equilibria. 4. United-Atom Description of Linear and Branched Alkenes and Alkylbenzenes. *J Phys Chem B* 104:8008–8016

122. Wick CD, Stubbs JM, Rai N et al (2005) Transferable potentials for phase equilibria. 7. United-atom description for nitrogen, amines, amides, nitriles, pyridine and pyrimidine. *J Phys Chem B* 109: 18974–18982
123. Boutard Y, Ungerer P, Teuler JM et al (2005) Extension of the anisotropic united atoms intermolecular potential to amines, amides and alkanols. Application to the problems of the 2004 Fluid Simulation Challenge. *Fluid Phase Equilib* 236:25–41
124. Contreras-Camacho RO, Ungerer P, Boutin A et al (2004) Optimized Intermolecular Potential for Aromatic Hydrocarbons Based on Anisotropic United Atoms. 1. Benzene. *J Phys Chem B* 108:14109–14114
125. Creton B, de Bruin T, Lachet V et al (2010) Extension of a Charged Anisotropic United Atoms Model to Polycyclic Aromatic Compounds. *J Phys Chem B* 114:6522–6530
126. Delhommelle J, Tschirwitz C, Ungerer P et al (2000) Derivation of an Optimized Potential Model for Phase Equilibria (OPPE) for Sulfides and Thiols. *J Phys Chem B* 104:4745–4753
127. Hadj-Kali MK, Gerbaud V, Joulia X et al (2008) Optimized intermolecular potential for nitriles based on anisotropic united atoms model. *J Mol Model* 14:571–580
128. Kranias S, Pattou D, Lévy B (2003) An optimized potential for phase equilibria calculation for ketone and aldehyde molecular fluids. *Phys Chem Chem Phys* 5:4175–4179
129. Nieto-Draghi C, Bonnaud P, Ungerer P (2007) Anisotropic United Atom Model Including the Electrostatic Interactions of Methylbenzenes. I. Thermodynamic and Structural Properties. *J Phys Chem C* 111:15686–15699
130. Ungerer P, le Beauvais C, Delhommelle J et al (2000) Optimization of the anisotropic united atoms intermolecular potential for n-alkanes. *J Chem Phys* 112:5499–5510
131. Nath SK, de Pablo JJ (2000) Simulation of vapor-liquid equilibria for branched alkanes. *Mol Phys* 98:231–238
132. Nath SK, Banaszak BJ, de Pablo JJ (2001) A new united atom force field for α -olefins. *J Chem Phys* 114:3612–3616
133. Nath SK, Khare R (2001) New force field parameters for branched hydrocarbons. *J Chem Phys* 115:10837–10844
134. Errington JR, Panagiotopoulos AZ (1999) New intermolecular potential models for benzene and cyclohexane. *J Chem Phys* 111:9731–9738
135. Damm W, Frontera A, Tirado-Rives J et al (1997) OPLS all-atom force field for carbohydrates. *J Comp Chem* 18:1955–1970
136. Jorgensen WL, McDonald NA (1998) Development of an all-atom force field for heterocycles. Properties of liquid pyridine and diazenes. *J Mol Struct THEOCHEM* 424:145–155
137. Kahn K, Bruice T (2001) Parameterization of OPLS-AA Force Field for the Conformational Analysis of Macrocyclic Polyketides. *J Comput Chem* 23:977–996
138. McDonald NA, Jorgensen WL (1998) Development of an All-Atom Force Field for Heterocycles. Properties of Liquid Pyrrole, Furan, Diazoles, and Oxazoles. *J Phys Chem B* 102:8049–8059
139. Rizzo RC, Jorgensen WL (1999) OPLS All-Atom Model for Amines: Resolution of the Amine Hydration Problem. *J Am Chem Soc* 121:4827–4836
140. MacKerell AD, Wiorkiewicz-Kuczera J, Karplus M (1995) An all-atom empirical energy function for the simulation of nucleic acids. *J Am Chem Soc* 117:11946–11975
141. Smit B, Karaborni S, Siepmann JI (1994) Computer simulations of vapor-liquid phase equilibria of n-alkanes. *J Chem Phys* 102:2126–2140
142. Toxvaerd S (1990) Molecular dynamics calculation of the equation of state of alkanes. *J Chem Phys* 93:4290–4296
143. Toxvaerd S (1997) Equation of state of alkanes II. *J Chem Phys* 107:5197–5204
144. Ferrando N, Lachet V, Teuler JM et al (2009) Transferable force field for alcohols and polyalcohols. *J Phys Chem B* 113:5985–5995
145. Lévy B, Enescu M (1998) Theoretical study of methylene blue: a new method to determine partial atomic charges; investigation of the interaction with guanine. *J Mol Struct THEOCHEM* 432:235–245
146. Glennon TM, Merz KM (1997) A carbohydrate force field for AMBER and its application to the study of saccharides to surface adsorption. *J Mol Struct THEOCHEM* 395–396:157–171

147. Yang L, Tan C, Hsieh MJ et al (2006) New-Generation Amber United-Atom Force Field. *J Phys Chem B* 110:13166–13176
148. van Gunsteren WF, Billeter SR, Eising AA et al (1996) Biomolecular Simulation: The GROMOS96 Manual and User Guide. Vdf Hochschulverlag, Zürich
149. Oostenbrink C, Villa A, Mark AE (2004) A Biomolecular Force Field Based on the Free Enthalpy of Hydration and Solvation: The GROMOS Force-Field Parameter Sets 53A5 and 53A6. *J Comput Chem* 25:1656–1676
150. Schuler LD, Daura X, van Gunsteren WF (2001) An improved GROMOS96 force field for aliphatic hydrocarbons in the condensed phase. *J Comput Chem* 22:1205–1218
151. Engelsen SB, Fabricius J, Rasmussen K (1994) The Consistent Force Field. 1. Methods and Strategies for Optimization of Empirical Potential Energy Functions. *Acta Chem Scand Ser A* 48:548–552
152. Engelsen SB, Fabricius J, Rasmussen K (1994) The Consistent Force Field. 2. An Optimized Set of Potential Energy Functions for the Alkanes. *Acta Chem Scand Ser A* 48:553–565
153. Jónsdóttir SO, Rasmussen K (2000) The consistent force field. Part 6: an optimized set of potential energy functions for primary amines. *New J Chem* 24:243–247
154. Shirts MR, Pitner JW, Swope WC et al (2003) Extremely precise free energy calculations of amino acid side chain analogs: Comparison of common molecular mechanics force fields for proteins. *J Chem Phys* 119:5740–5761
155. Guvench O, MacKerell AD (2008) Comparison of Protein Force Fields for Molecular Dynamics Simulations. In: Kukol A (ed) *Molecular Modeling of Proteins*. Humana Press, New York
156. Mackerell AD (2004) Empirical force fields for biological macromolecules: Overview and issues. *J Comput Chem* 25:1584–1604
157. Ponder JW, Case DA (2003) Force fields for protein simulations. *Protein Simul* 66:27–85
158. Price DJ, Brooks CL (2002) Modern protein force fields behave comparably in molecular dynamics simulations. *J Comput Chem* 23:1045–1057
159. Yoda T, Sugita Y, Okamoto Y (2004) Comparisons of force fields for proteins by generalized-ensemble simulations. *Chem Phys Lett* 386:460–467
160. Hobza P, Hubálek F, Kabeláč M et al (1996) Ability of empirical potentials (AMBER, CHARMM, CVFF, OPLS, Poltev) and semi-empirical quantum chemical methods (AM1, MNDO/M, PM3) to describe H-bonding in DNA base pairs; comparison with ab initio results. *Chem Phys Lett* 257:31–35
161. Yeh IC, Hummer G (2002) Peptide Loop-Closure Kinetics from Microsecond Molecular Dynamics Simulations in Explicit Solvent. *J Am Chem Soc* 124:6563–6568
162. Stortz CA, Johnson GP, French AD et al (2009) Comparison of different force fields for the study of disaccharides. *Carbohydr Res* 344:2217–2228
163. Patra M, Karttunen M (2004) Systematic comparison of force fields for microscopic simulations of NaCl in aqueous solutions: Diffusion, free energy of hydration and structural properties. *J Comput Chem* 25:678–689
164. Patel S, Brooks CL (2004) CHARMM Fluctuating Charge Force Field for Proteins: I Parameterization and Application to Bulk Organic Liquid Simulations. *J Comput Chem* 25:1–15
165. Gao J, Habibollazadeh D, Shao L (1995) A Polarizable Intermolecular Potential Function for Simulation of Liquid Alcohols. *J Phys Chem* 99:16460–16467
166. Gao J, Pavelites J, Habibollazadeh D (1996) Simulation of Liquid Amides Using a Polarizable Intermolecular Potential Function. *J Phys Chem* 100:2689–2697
167. Xie W, Pu J, MacKerell AD et al (2007) Development of a polarizable intermolecular potential function (PIPF) for liquid amides and alkanes. *J Chem Theory Comput* 3:1878–1889
168. Ponder JW, Wu C, Ren P (2010) Current Status of the AMOEBA Polarizable Force Field. *J Phys Chem B* 114:2549–2564
169. Martin MG (2006) Comparison of the AMBER, CHARMM, COMPASS, GROMOS, OPLS, TraPPE and UFF force fields for prediction of vapor-liquid coexistence curves and liquid densities. *Fluid Phase Equilib* 248:50–55
170. Dellis D, Samios J (2010) Molecular force field investigation for Sulfur Hexafluoride: A computer simulation study. *Fluid Phase Equilib* 291:81–89

171. Fernandez GA, Vrabec J, Hasse H (2005) Shear Viscosity and Thermal Conductivity of Quadrupolar Real Fluids from Molecular Simulation. *Mol Sim* 31:787–793
172. Fernandez GA, Vrabec J, Hasse H (2006) Shear Viscosity and Thermal Conductivity of Dipolar Real Fluids from Molecular Simulation. *Cryogenics* 46:711–717
173. Fermeglia M, Ferrone M, Priol S (2003) Development of an all-atoms force field from ab initio calculations for alternative refrigerants. *Fluid Phase Equilib* 210:105–116
174. Huang YL, Heilig M, Hasse H et al (2010) VLE of Hydrogen Chloride, Phosgene, Benzene, Chlorobenzene, Ortho-Dichlorobenzene and Toluene by Molecular Simulation. *AIChE J*. 57:1043–1060
175. Hunt PA (2006) The simulation of imidazolium-based ionic liquids. *Mol Simul* 32:1–10
176. Liu X, Zhang S, Zhou G et al (2006) New Force Field for Molecular Simulation of Guanidinium-Based Ionic Liquids. *J Phys Chem B* 110:12062–12071
177. Hellmann R, Bich E, Vogel E (2008) *Ab initio* intermolecular potential energy surface and second pressure virial coefficients of methane. *J Chem Phys* 128:214303
178. Hellmann R, Bich E, Vogel E (2008) *Ab initio* potential energy curve for the neon atom pair and thermophysical properties of the dilute neon gas. I. Neon-neon interatomic potential and rovibrational spectra. *Mol Phys* 106:133–140
179. Domański K, Kitao O, Nakanishi K (1994) A New Potential Model for Carbon Dioxide from Ab Initio Calculations. *Mol Simul* 12:343–353
180. Frenkel D, Smit B (2002) *Understanding molecular simulation: from algorithms to applications*, 2nd edn. Elsevier, San Diego
181. Panagiotopoulos AZ (1996) Current advances in Monte Carlo methods. *Fluid Phase Equilib* 116:257–266
182. Theodorou DN (2010) Progress and Outlook in Monte Carlo Simulations. *Ind Eng Chem Res* 49:3047–3058
183. Allen MP, Tildesley DJ eds (1993) *Computer Simulation in Chemical Physics*. Kluwer Academic Publishers, Dordrecht
184. Amar JG (2006) *The Monte Carlo Method in Science and Engineering*. *Comput Sci Eng* 8:9–19
185. Baus M, Rull LF, Ryckaert JP eds (1995) *Observation and Prediction of Phase Transitions in Complex Fluids*. Kluwer Academic Publishers, Dordrecht
186. Valleau JP (1991) Density-scaling: A new Monte Carlo technique in statistical mechanics. *J Comput Phys* 96:193–216
187. Ferrenberg AM, Swendsen RH (1988) New Monte Carlo technique for studying phase transitions. *Phys Rev Lett* 61:2635–2638
188. Ferrenberg AM, Swendsen RH (1989) Optimized Monte Carlo data analysis. *Phys Rev Lett* 63:1195–1198
189. Kofke DA (1993) Gibbs-Duhem integration: a new method for direct evaluation of phase coexistence by molecular simulation. *Mol Phys* 78:1331–1336
190. Vrabec J, Hasse H (1995) Vapour liquid equilibria of mixtures from the NpT plus test particle method. *Mol Phys* 85:781–792
191. Boda D, Kristóf T, Liszi J et al (2001) A new simulation method for the determination of phase equilibria in mixtures in the grand canonical ensemble. *Mol Phys* 99:2011–2022
192. Vrabec J, Hasse H (2002) Grand Equilibrium: vapour-liquid equilibria by a new molecular simulation method. *Mol Phys* 100:3375–3383
193. Panagiotopoulos AZ (1987) Direct determination of phase coexistence properties of fluids by Monte Carlo simulation in a new ensemble. *Mol Phys* 61:813–826
194. Panagiotopoulos AZ (2000) Monte Carlo methods for phase equilibria of fluids. *J Phys: Condens Matter* 12:25–52
195. de Pablo JJ, Yan Q, Escobedo FA (1999) Simulation of phase transitions in fluids. *Annu Rev Phys Chem* 50:377–411
196. Lamm MJ, Hall CK (2001) Molecular Simulation of Complete Phase Diagrams for Binary Mixtures. *AIChE J* 47:1664–1675
197. Johnson JK, Panagiotopoulos AZ, Gubbins KE (1994) Reactive canonical Monte Carlo: a new simulation technique for reacting or associating fluids. *Mol Phys* 81:717–733

198. Smith WR, Triska B (1994) The reaction ensemble method for the computer simulation of chemical and phase equilibria I. Theory and basic examples. *J Chem Phys* 100:3019–3027
199. Kiyohara K, Spyriouni T, Gubbins KE et al (1996) Thermodynamic scaling Gibbs ensemble Monte Carlo: a new method for determination of phase coexistence properties of fluids. *Mol Phys* 89:965–974
200. Briano JG, Glandt ED (1984) Statistical thermodynamics of polydisperse fluids. *J Chem Phys* 80:3336–3343
201. Kofke DA, Glandt ED (1988) Monte Carlo simulation of multicomponent equilibria in a semigrand canonical ensemble. *Mol Phys* 64:1105–1131
202. Potoff JJ, Panagiotopoulos AZ (2000) Surface tension of the three-dimensional Lennard-Jones fluid from histogram-reweighting Monte Carlo simulations. *J Chem Phys* 112:6411–6416
203. Singh JK, Errington JR (2006) Calculation of Phase Coexistence Properties and Surface Tensions of n-Alkanes with Grand-Canonical Transition-Matrix Monte Carlo Simulation and Finite-Size Scaling. *J Phys Chem B* 110:1369–1376
204. Ungerer P, Boutin A, Fuchs AH (1999) Direct calculation of bubble points by Monte Carlo simulations. *Mol Phys* 97:523–539
205. Escobedo FA (1998) Novel pseudoensembles for simulation of multicomponent phase equilibria. *J Chem Phys* 108:8761–8772
206. van der Vegt NFA, Briels WJ, Wessling M et al (1999) The sorption induced glass transition in amorphous glassy polymers. *J Chem Phys* 110:11061–11069
207. Widom B (1963) Some topics in the theory of fluids. *J Chem Phys* 39:2808–2812
208. Lyubartsev AP, Martsinovski AA, Shevkunov SV et al (1992) New approach to Monte Carlo calculation of the free energy: Method of expanded ensembles. *J Chem Phys* 96:1776–1785
209. Nezbeda I, Kolafa J (1991) A New Version of the Insertion Particle Method for Determining the Chemical Potential by Monte Carlo Simulation. *Mol Simul* 5:391–403
210. Vrabec J, Kettler M, Hasse H (2002) Chemical potential of quadrupolar two-centre Lennard-Jones fluids by gradual insertion. *Chem Phys Lett* 356:431–436
211. Maginn EJ, Bell AT, Theodorou DN (1995) Sorption Thermodynamics, Siting, and Conformation of Long n-Alkanes in Silicalite as Predicted by Configurational-Bias Monte Carlo Integration. *J Phys Chem* 99:2057–2079
212. Theodorou DN (2006) A reversible minimum-to-minimum mapping method for the calculation of free-energy differences. *J Chem Phys* 124:034109
213. Kofke DA, Cummings PT (1997) Quantitative comparison and optimization of methods for evaluating the chemical potential by molecular simulation. *Mol Phys* 92:973–996
214. Murad S, Gupta S (2000) A simple molecular dynamics simulation for calculating Henry's constant and solubility of gases in liquids. *Chem Phys Lett* 319:60–64
215. Sadus RJ (1997) Molecular simulation of Henry's constant at vapor-liquid and liquid-liquid phase boundaries. *J Phys Chem B* 101:3834–3838
216. Shing KS, Gubbins KE, Lucas K (1988) Henry constants in nonideal fluid mixtures. Computer simulation and theory. *Mol Phys* 65:123–1252
217. Green MS (1954) Markoff Random Processes and the Statistical Mechanics of Time-Dependent Phenomena. II. Irreversible Processes in Fluids. *J Chem Phys* 22:398–414
218. Kubo R (1957) Statistical-Mechanical Theory of Irreversible Processes. I. General Theory and Simple Applications to Magnetic and Conduction Problems. *J Phys Soc Jpn* 12:570–586
219. Ciccotti G, Frenkel D, McDonald IR (1987) *Simulation of Liquids and Solids*. North-Holland, Amsterdam
220. Rowley RL, Painter MM (1997) Diffusion and Viscosity Equations of State for a Lennard-Jones Fluid Obtained from Molecular Dynamics Simulations. *Int J Thermophys* 18:1109–1121
221. Hoover WG, Evans DJ, Hickman RB et al (1980) Lennard-Jones triple-point bulk and shear viscosities. Green-Kubo theory, Hamiltonian mechanics, and nonequilibrium molecular dynamics. *Phys Rev A* 22:1690–1697
222. Ladd AJC (1984) Equations of motion for non-equilibrium molecular dynamics simulations of viscous flow in molecular fluids. *Mol Phys* 53:459–463

223. Lees AW, Edwards SF (1972) The computer study of transport processes under extreme conditions. *J Phys C* 5:1921–1929
224. Evans DJ, Morris GP (1990) *Statistical Mechanics of Nonequilibrium Liquids*. Academic Press, London
225. Cummings PT, Evans DJ (1992) Nonequilibrium Molecular Dynamics Properties and Non-Newtonian Fluid Approaches to Transport Rheology. *Ind Eng Chem Res* 31:1237–1252
226. Müller-Plathe F (1997) A simple nonequilibrium molecular dynamics method for calculating the thermal conductivity. *J Chem Phys* 106:6082–6085
227. Müller-Plathe F, Bordat P (2004) Reverse Non-equilibrium Molecular Dynamics. *Lect Notes Phys* 640:310–326
228. Chen T, Smit B, Bell AT (2009) Are pressure fluctuation-based equilibrium methods really worse than nonequilibrium methods for calculating viscosities?. *J Chem Phys* 131:246101
229. Sadus RJ (2002) *Molecular Simulation of Fluids: Theory, Algorithms and Object-Oriented*. Elsevier, Amsterdam
230. <http://www.charmm.org/>
231. Smith W, Yong CW, Rodger PM (2002) DL-POLY: Application to molecular simulation. *Mol Simul* 28:385–471
232. Hess B, Kutzner C, van der Spoel D et al (2008) GROMACS 4: Algorithms for Highly Efficient, Load-Balanced, and Scalable Molecular Simulation. *J Chem Theory Comput* 4:435–447
233. Plimpton S (1995) Fast Parallel Algorithms for Short-Range Molecular Dynamics. *J Comp Phys* 117:1–19
234. <http://www.vscht.cz/fch/software/macsimus/index.html>
235. Refson K (2000) Moldy: a portable molecular dynamics simulation program for serial and parallel computers. *Comput Phys Commun* 126:309–328
236. Deublein S, Eckl B, Stoll J et al (2011) ms2: A Molecular Simulation Tool for Thermodynamic Properties. *Comput Phys Commun*, in press
237. Phillips JC, Braun R, Wang W et al (2005) Scalable molecular dynamics with NAMD. *J Comput Chem* 26:1781–1802
238. Ponder JW (2009) TINKER: Software Tools for Molecular Design, 5.0. Washington University School of Medicine, Saint Louis
239. Müller-Plathe F (1993) YASP: A molecular simulation package. *Comput Phys Commun* 78:77–94
240. <http://molsim.chem.uva.nl/bigmac/bigmac.html>
241. Jorgensen WL, Tirado-Rives J (2005) Molecular modeling of organic and biomolecular systems using BOSS and MCPRO. *J Comput Chem* 26:1689–1700
242. <http://kea.princeton.edu/jerring/gibbs>
243. <http://www.materialsdesign.com/medea/medea-gibbs>
244. <http://towhee.sourceforge.net/>
245. Jorgensen WL, Ibrahim M (1980) The Structure and Properties of Liquid Ammonia. *J Am Chem Soc* 102:3309–3315
246. Hinchliffe A, Bounds DG, Klein ML et al (1981) Intermolecular potentials for ammonia based on SCF-MO calculations. *J Chem Phys* 74:1211–1217
247. Sagarik KP, Ahlrichs R, Brode S (1986) Intermolecular potentials for ammonia based on the test particle mode and the coupled pair functional method. *Mol Phys* 57:1247–1264
248. Caillol JM, Levesque D, Weis JJ (1987) A theoretical study of a polar-polarizable model for liquid ammonia. *Mol Phys* 62:1225–1238
249. Mansour KA, Murad S (1987) A Computer Simulation Study of Fluid Ammonia. *Fluid Phase Equilib* 37:305–325
250. Hannongbua SV, Ishida T, Spohr E et al (1988) Molecular Dynamics Study of a Lithium Ion in Ammonia. *Z Naturforsch* 43a:572–582
251. Gao J, Xia X, George TF (1993) Importance of Bimolecular Interactions in Developing Empirical Potential Functions for Liquid Ammonia. *J Phys Chem* 97:9241–9247
252. Kristóf T, Vorholz J, Liszi J et al (1999) A simple effective pair potential for the molecular simulation of the thermodynamic properties of ammonia. *Mol Phys* 97:1129–1137

253. Zhang L, Siepmann JI (2010) Development of the TraPPE force field for ammonia. *Collect Czech Chem Commun* 75:577–591
254. Benedict WS, Plyler EK (1957) Vibration-rotation bands of ammonia: II. The molecular dimensions and harmonic frequencies of ammonia and deuterated ammonia. *Can J Phys* 35: 1235–1241
255. Tillner-Roth R, Harms-Watzenberg F, Baehr HD (1993) Eine neue Fundamentalgleichung für Ammoniak. *DKV-Tagungsbericht* 20:167–181
256. Gross T, Buchhauser J, Price W et al (1997) The p,T-dependence of self-diffusion in fluid ammonia. *J Mol Liq* 73:433–444
257. Tufeu R, Ivanov DY, Garrabas Y et al (1984) Thermal Conductivity of Ammonia in a Large Temperature and Pressure Range Including the Critical Region. *Ber Bunsenges Phys Chem* 88:422–427
258. Schnabel T, Vrabec J, Hasse H (2005) Henry's Law Constants of Methane, Nitrogen, Oxygen and Carbon Dioxide in Ethanol from 273 to 498 K: Prediction from Molecular Simulation. *Fluid Phase Equilib* 233:134–143, 236:272, 239:125–126
259. Hayduk W, Cheng SC (1970) Solubilities of ethane and other gases in normal paraffin solvents. *Can J Chem Eng* 48:93–99
260. Kierzkowska-Pawlak H, Zarzycki R (2002) Solubility of carbon dioxide and nitrous oxide in water + methyldiethanolamine and ethanol + methyldiethanolamine solutions. *J Chem Eng Data* 47:1506–1509
261. Kunerth W (1922) Solubility of carbon dioxide and nitrous oxide in certain solvents. *Phys Rev* 19:512–524
262. Luehring P, Schumpe A (1989) Gas solubilities (hydrogen, helium, nitrogen, carbon monoxide, oxygen, argon, carbon dioxide) in organic liquids at 293.2 K. *J Chem Eng Data* 34:250–252
263. Postigo MA, Katz M (1987) Solubility and thermodynamics of carbon dioxide in aqueous ethanol solutions. *J Solution Chem* 16:1015–1024
264. Takahashi M, Kobayashi Y, Takeuchi H (1982) Diffusion coefficients and solubilities of carbon dioxide in binary mixed solvents. *J Chem Eng Data* 27:328–331
265. Tokunaga J, Nitta T, Katayama T (1969) Solubility of carbon dioxide in aqueous alcohol solutions. Methanol-water, ethanol-water systems. *Chem Eng Jpn* 33:775–779
266. Fredenslund A, Sather GA (1970) Gas-Liquid Equilibrium of the Oxygen-Carbon Dioxide System. *J Chem Eng Data* 15:17–22